# BRNO UNIVERSITY OF TECHNOLOGY
VYSOKÉ UČENÍ TECHNICKÉ V BRNĚ

## FACULTY OF CIVIL ENGINEERING
FAKULTA STAVEBNÍ

## INSTITUTE OF STRUCTURAL MECHANICS
ÚSTAV STAVEBNÍ MECHANIKY

## ANALYSIS OF MIXED MODE I/II FAILURE OF SELECTED STRUCTURAL CONCRETE GRADES
ANALÝZA KOMBINOVANÉHO MÓDU I/II NAMÁHÁNÍ VYBRANÝCH TŘÍD BETONU

## SHORTENED VERSION OF DOCTORAL THESIS
ZKRÁCENÁ VERZE DIZERTAČNÍ PRÁCE

**AUTHOR**             Ing. Petr Miarka
AUTOR PRÁCE

**SUPERVISOR**         doc. Ing. Stanislav Seitl, Ph.D.,
ŠKOLITEL

**BRNO 2021**

# TABLE OF CONTENT

# Introduction

The last two decades have witnessed a considerable progress towards the design, construction and maintenance of concrete structures which concerned both economic and environmental impacts of these structures on the environment to be built in. These two primary demands can be met by the development and eventual use of a material which exhibits higher mechanical performance and simultaneously has a lower environmental impact. The use of high-strength concrete (HSC) [1] allows for a material reduction in the structure's cross-sectional dimensions, while high-performance concrete (HPC) [2, 3] exhibits higher long-term performance and durability of the structure. The structures (e.g. bridges or beams) to be built from such materials can benefit from a greater span length, a shallow beam cross-section and an extended service lifetime.

The modern HPC and HSC mixtures used in the construction consume less natural resources, i.e. raw materials for cement production, aggregates, water, and their mixture typically contains less cement (lower $CO_2$ emission) [4, 5], while the mechanical and/or durability performance is enhanced. This results in a reduction of the production cost (subtle structural element) and $CO_2$ emissions (lower cement content). This reduction of natural resources is done by composing a concrete mixture which contains mineral admixtures, i.e. supplementary cementitious materials (SCM) like silica fume [6], ground granulated blast furnace slag [7], fly ash, or it can include natural pozzolans, e.g. pumice [8], metakaolin or zeolite [9] etc.

Regarding the strict $CO_2$ emission requirements, the concrete technology developed completely new cement free materials due to new sustainable binders. These cement free materials replaced cement by an alkali activated binder. Thus, the concrete made with such binder is called an alkali-activated concrete (AAC) [10, 11] or sometimes referred as geopolymers. In this case the grains hold together by reaction alkali-activators NaOH or KOH [12], which activate the precursors. The precursors can be, e.g. grinded and quenched blast furnace slags [10], various slags from ferrous and non-ferrous metallurgy [10], Fe-rich clays [13], ground coal bottom ash [14] and kaolin [15].

On the other hand, subtle structures made of the new materials drew attention to a comprehensive structural analysis, which resulted in the use of advanced material models as implemented in the finite element method (FEM) software. This overcame a traditional, sometimes empirical design methods mentioned in the standards [16, 17] or in recommendations [18], due to the lack of knowledge of the material's or structural response and may not be sufficient to provide an effective structural design.

Standard tests provide information about the compressive $f_c$ or the tensile $f_t$ strength, the Young's modulus $E$ and the bulk density $\rho$. Advanced material behaviour can be described using fracture mechanical parameters (FMP) such as the fracture toughness $K_{IC}$, the fracture energy $G_f$, and the crack mouth opening displacement ($CMOD$) or the crack mouth opening sliding ($CMOS$). The fracture energy $G_f$ is considered as an important material parameter, which depends on the aggregate size and the quality of the concrete Thorough knowledge of this behaviour is required as it is the most important parameter in the post peak behaviour of the material in tension as it is closely related to crack initiation; it also determines the durability within the structure's lifetime.

Due to the structural geometry, the loading conditions or the construction technology, concrete structures and their structural elements are typically subjected to a combination of bending and shear loads. The fracture process in such structural elements can be divided into actions from tensile loads (mode I), shear loads (mode II) or any combination of tensile and shear loads (mixed mode I/II).

Even a simply supported beam with distributed load (see Figure 1(a)) carries such a combination of mode I and mode II load. If the stress distribution is plotted in principal stresses, one can find the location of the highest tensile mode I stresses and highest mode II shear stresses, which produce the main failure mechanism (transverse tension) of concrete structures. The highest normal mode I stress are located in the mid span of the beam, while the highest shear mode II stresses are located above support. These points attract most attention in the design process of the concrete beam.



(a)



(b)
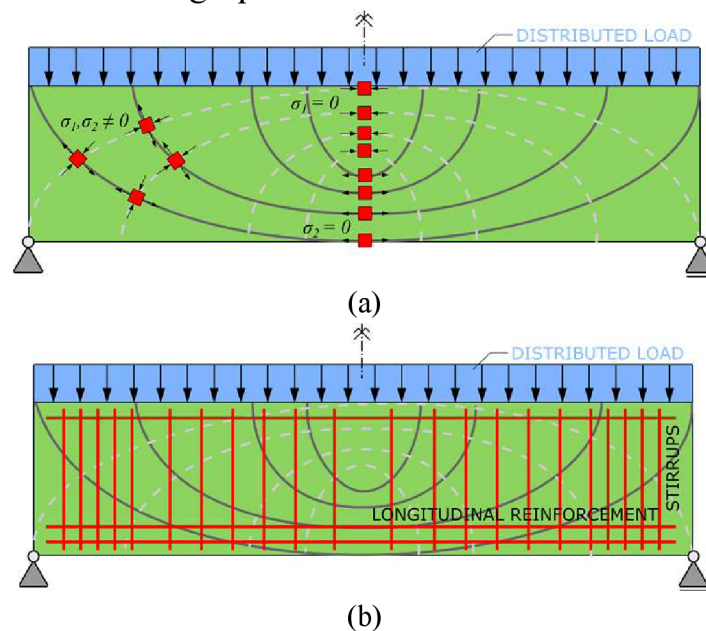
**Figure 1:** Principal stress $\sigma_1$ and $\sigma_2$ trajectories on the simply supported beam with a distributed load (a) and designed steel reinforcement (b).

Nevertheless, there is a location with a combination of tensile and shear stress which produces mixed mode I/II crack initiation. This fact is unintentionally omitted in studies, and in practice this weakest material point is strengthened using shear reinforcement – stirrups [16] (see Figure 1(b)). However, static or cyclic load [19, 20] can lead to micro-cracks in the concrete cover layer which propagate and increase in size until final failure occurs [21, 22]. This often leads to reinforcement exposure, and thus to the reduction of the total service lifetime [23].

Despite the improved strength and performance, the HPC concrete is prone to forming micro-cracks, which propagate and increase in size throughout the cover layer. This leads to a significant durability issue as the steel reinforcement is exposed to weather conditions [23-27]. Moreover, these weather conditions are often highly aggressive (de-icing salts or a marine environment) and assist to accelerate the steel reinforcement corrosion which results into the structure's premature degradation [28, 29].

Typically, the fracture mechanical parameters are evaluated from recommendations, where the specimens are prismatic plates, beams or cubes with rectangular/square cross-section e.g. the compact tension (CT) test [30], the three-point or the four-point bending (3PB, 4PB) test [31, 32] (Figure 2(a)) or the wedge splitting test (WST) [33] (Figure 2(b)).
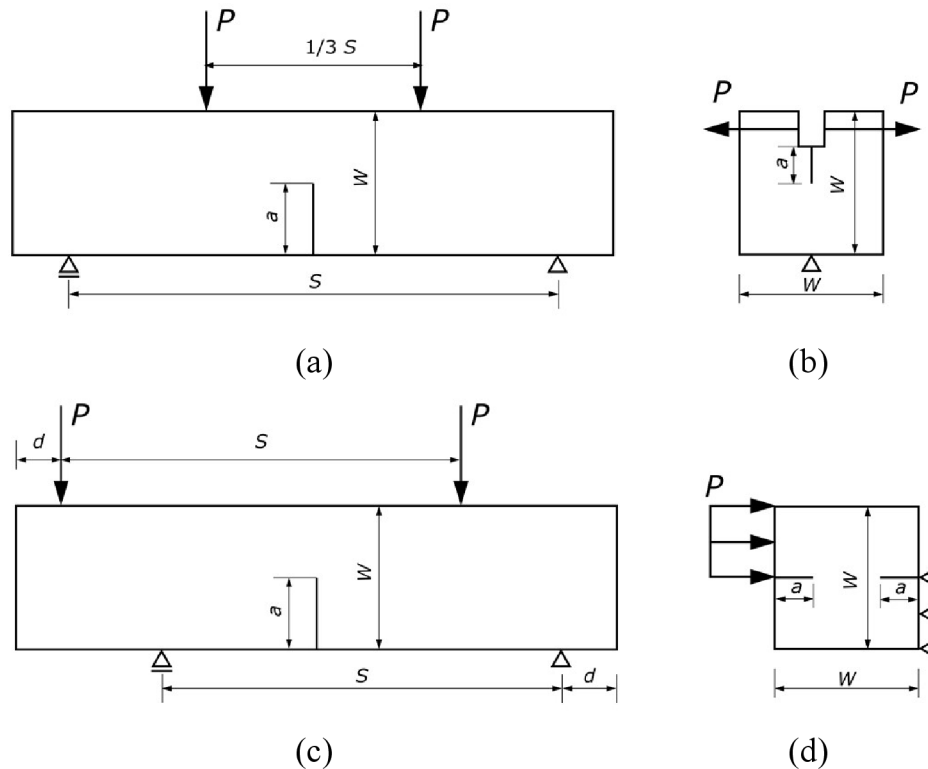


**Figure 2:** Comparison of test specimens for fracture mechanical tests – for mode I: four-point bending test (a) and wedge splitting test (b), for mode II: eccentric asymmetric four-point bending test (c) and double-edge notched specimen (d).

These tests provide information about the fracture behaviour under the tensile mode I. Information about shear mode II is provided by tests such as the eccentric asymmetric four-point bending test (EA4PBT) [34] (Figure 2(c)) or the double-edge notched specimen test (DENS) [35] (Figure 2(d)).

All of these tests can be used in the design of new structures as samples can be cast together with the structure in any shape and size. In contrast, for a structure to be renovated, a core has to be drilled, which removes a cylindrical material sample from the investigated structure. Reshaping a cylindrical sample into a prism is ineffective and expensive.

The Brazilian disc test with central notch (BDCN) [36-38] (Figure 3(a)) or semi-circular bend (SCB) test [39-41] (Figure 3(b)) suggest such an application and provide information about tensile mode I, combination of tensile and shear mixed mode I/II and pure shear mode II crack initiation conditions. The investigation of the mixed mode I/II is done by inclining the initial notch against the load position. This allows the fracture mechanical test to be performed under relatively simple experimental conditions using a standard compressive testing apparatus with sufficient load capacity.



(a)                                    (b)
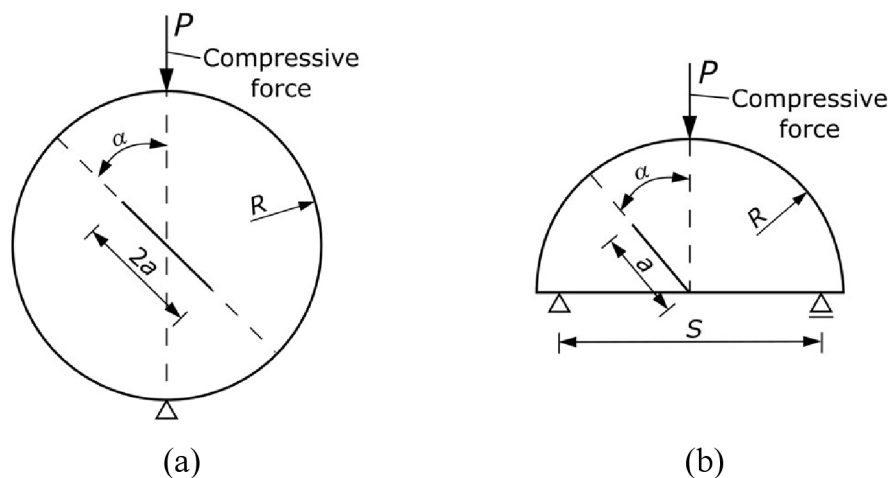
**Figure 3:** Comparison of two fracture mechanical test made form core-drill sample – Brazilian disc with central notch (a) and semi-circular bend test (b).

The mixed-mode I/II fracture condition is achieved, in both specimens, by inclining the initial notch against the loading position. This fact reduces demands on the experiments, as a common testing apparatus with sufficient load capacity can be used. On the other hand, the preparation of the notches is more labour intensive and requires a skilled worked compared to traditional prismatic specimens.

## Problem Statement

Concrete material is profoundly used in almost every civil engineering structures, which are part of the important infrastructure, already built or to be built. Technological progress and increasing ambitious, sometimes critical, requirements on the new structure have launched a complete change in the concrete technology and construction. Such requirements can be split into two main branches.

The first demand concerns environmental impacts with increased awareness of the $CO_2$ emissions reduction of whole cement industry. Consequently, the focus was placed on various mitigation strategies, which include variety of approaches e.g. fuel substitution, use of alternative raw materials, and use of material substitutes [5]. The other demand reflects both a need to repair current infrastructure, e.g. roads, bridges, buildings, where old system have lost its functionally and a need to build new infrastructure to expand current system. This aims to reduce structure's and maintenance costs over the designed structure's lifetime. Cost reduction potential is expected not only from the more environmental cement production but also from more efficient use of cement in concrete and in its application in construction industry. This implies the need for corresponding standards and quality measures to safeguard the concrete construction along the structure's life [4].

Such demands have gradually led to the development of new concrete mixtures with improved mechanical properties and structural response. However, the main failure of concrete structure is due to development of micro-cracks which are progressively increasing in size over the time and result in the major macro-crack. This process affects the structure's durability and reduces the structure's life. Hence, the analysis of the crack initiation and propagation in concrete material is at most interest to reduce the additional cost or worse the structure demolition. These cracks can initiate due to several reasons but mainly from the action of external loads i.e. static or cyclic. Static loads are present during whole structural activity and usually lead to single damage initiation, while the cyclic loads repeat themselves, which can result in the longer damage initiation process. Typically, it takes years for damage to be spotted and located on the structure. From the linear elastic fracture mechanics (LEFM) viewpoint, this process is called mixed mode I/II crack initiation and it can consider actions from both static and fatigue loads.

Experimental verification of the analytical formulas mentioned in fracture mechanical handbooks, can be done by employing the digital image correlation (DIC) method [42]. The DIC technique captures deformations fields of the specimen that arise due to the applied load during experimental testing. Such displacement fields captured in the close

vicinity of the crack tip measured under the various mixed-mode I/II loading conditions is used to calculate fracture mechanical parameters.

The above-mentioned research objectives and standards mostly focus on the crack initiation and crack path prediction. However, the structure is exposed to combination of environmental and physical loads within the structure lifetime. While the research of the actual effect of soluble chlorides on the crack development is unique, especially considering mixed mode I/II loading conditions. Therefore, the relationship between the FMPs of the cement-based composite/concrete and its resistance to chloride penetration is a very interesting problem to investigate together with the influence of the chloride penetration depth on the load bearing capacity of the cross-section. Thus, it is of the most interest to investigate the influence of the aggressive chloride environment on the fracture toughness and fracture resistance under the mixed mode I/II loading conditions.

This lack of knowledge of the material fracture resistance to the mixed-mode I/II has led to the present study.

## Goals

In order to achieve a correct and reliable application of the mixed mode I/II fracture resistance, this work aims to give better insight into crack initiation and failure mechanism of the mixed mode I/II load, which has been studied numerically and verified experimentally.

The main objectives of the presented thesis are:

    a)   Deepen the understanding of mixed mode I/II crack initiation conditions for concrete materials.

    b)   To analyse and validate the use of analytical formulas by employment of the digital image correlation technique.

    c)   Deepen the knowledge of governing role of the critical distance $r_C$ on the mixed-mode I/II crack initiation process.

    d)   To establish the connection among the experimental results and the numerical simulation throughout appropriate material model.

    e)   To study the influence of the aggressive environment on the fracture resistance of under the mixed mode I/II load.

    f)   To verify applicability of the higher order terms of the Williams's expansion on the concrete materials.

    g)   Analyse the stress and strain fields by non-linear numerical analysis in order to give insights to crack initiation conditions under the mixed mode I/II.

## Methods

Experimental research is carried out, considering various types of concrete mixtures, e.g. C50/60, two kinds of HPC, AAC and HSC. These mixtures were compared to the commonly used C 50/60 concrete grade in the fabrication of the precast concrete structural elements. Firstly, the mechanical tests were carried out to determinate the material's performance. Furthermore, comprehensive numerical simulation by finite elements models was carried out to analyse the crack initiation and failure mechanism under the mixed mode I/II load and to obtain analytical formulas for the used geometry. For this, two different software was used i.e. ANSYS and Abaqus, nonetheless the obtained results were not compared in between due to the licence agreement. Afterwards, these concrete mixtures were tested to obtain mixed mode I/II fracture resistance curves. In addition to this, the HPC mixture was studied by the digital image correlation technique to verify the analytical formulas given by the literature and to analyse the failure mechanism of the mixed mode I/II loading. Lastly the HPC mixture has been exposed to the aggressive environment to study the influence of aggressive environment on the FMPs.

This experimental research and mixture development were done in close cooperation with the ŽPSV s.r.o. company, Institute of Physics of Materials of the Czech Academy of the Sciences, Department of Building Materials and Diagnostics of Structures of the Faculty of Civil Engineering of Technical University of Ostrava, Department of Structural Engineering and Building Materials at Ghent University and Department of Civil and Materials Engineering at University of Malaga.

# 1  Theoretical Background

Concrete cracking is a very complex mechanism, which is substantially different from the cracking behaviour of the other materials used in civil engineering industry. Over the last few decades, suitable fracture mechanical models, together with test configuration have been established to determinate the fracture mechanical parameters of concrete, which belongs to quasi-brittle materials.

## 1.1  Linear Elastic Fracture Mechanics

The fundamental concepts of fracture mechanics have been established in 1920 by Griffith [43], in which the unstable crack propagation based on the first law of thermodynamics. This hypothesis correctly predicted failure, if applied to glass specimen. If applied to other material, like to ductile metals, Griffith's approach has some shortcomings. Therefore, Irwin [44] developed a modified version of the Griffith's energy-based approach. Irwin in his modifications showed that the stresses and displacements near the crack tip can be described by a single constant, related to the energy release rate, called the stress intensity factor (SIF). During the same period of time, Williams [45] and [46] applied a somewhat different technique to derive crack tip solutions with results essentially identical to Irwin's results. These analyses are restricted to structures whose global behaviour is linear elastic and obey Hooke's law, therefore this research field is call linear elastic fracture mechanics shortly - LEFM.

This thesis, in most of its parts, deals with the LEFM concept and uses the solution prosed by Williams [45]. The literature dedicated to LEFM recognize three basic modes of the crack opening [47, 48]. These crack opening modes are showed in Figure 4.
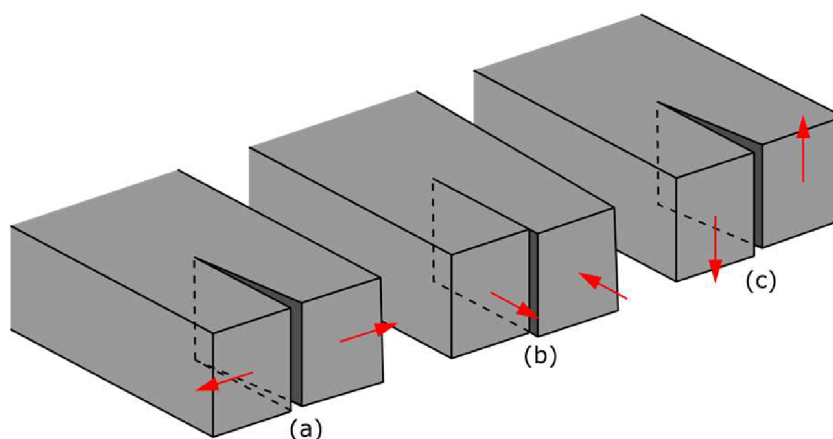


**Figure 4:** Basic crack opening modes recognized by LEFM – (a) -Mode I, the tensile opening mode, (b) – Mode II, the in-plane shear mode and (c) – Mode III, the out-plane shear mode.

Mode I, the opening mode is when the opposing crack faces/surfaces move directly apart due to tensile load, Figure 4(a). Mode II, so-called the in-plane shear, is present when the crack faces/surfaces move over each other perpendicular to the crack front, Figure 4(b). The Mode III, so-called the out-plane shear is present when the crack surfaces move over from each other parallel to the crack front, Figure 4(c). Any combination of such a loading mode is called mixed mode loading conditions. Further in this thesis the crack analysis is limited to the two-dimensional (2D) problem with focus set to analyse the combination of tensile mode I and shear mode II i.e. the mixed mode I/II loading conditions.

Concrete is composite material composed of fine and coarse aggregates bounded together with a cement matrix that hardens over time. Thus, fracture of concrete is highly complex process that still poses challenge in composing experimental setup, numerical modelling, and concrete technology. Microstructure of concrete is highly heterogenous due to presence of flaws, such as pores, inclusions, and micro-cracks. These micro-cracks are locations, which can promote debonding of aggregate particles from the cement matrix. Further coalescence of these microscopic cracks due to external loading inevitably leads to observable macro-cracking. The cracks are not only affecting the aesthetic look and durability, but possibly jeopardizing the structural stability, as well. However, concrete cracking is inherent to the material and it does not necessarily result in structural failure; stabilized cracks are not dangerous [49]. It is important to fully understand the material's fracture and failure behaviour in order to make correct judgment of this.

To introduce main differences in the fracture process of concrete material, it is most explanatory to show concrete material's response to the actions of external tensile load. This comparison is usually expressed by the applied load versus produced deformation ($P$-$\delta$) diagram. Concrete's response to the load, so-called quasi-brittle.

The region in which the quasi-brittle material undergoes softening damage (tearing), featured by progressive micro-cracking, is called the fracture process zone (FPZ). This softening, in the FPZ is result from the micro-cracking of concrete material. The presence of FPZ is the main reason for the deviation of the concrete behaviour from the LEFM prediction. The FPZ is formed, when micro-cracks are propagating and later coalescing into observable macro-crack. In this zone, due to the existence of micro-cracks concrete material progressively softens [49]. This above-referred phenomenon of response to tensile load can be examined in more detail if the crack tip situation is shown in Figure 5.

(a)                                                        (b)
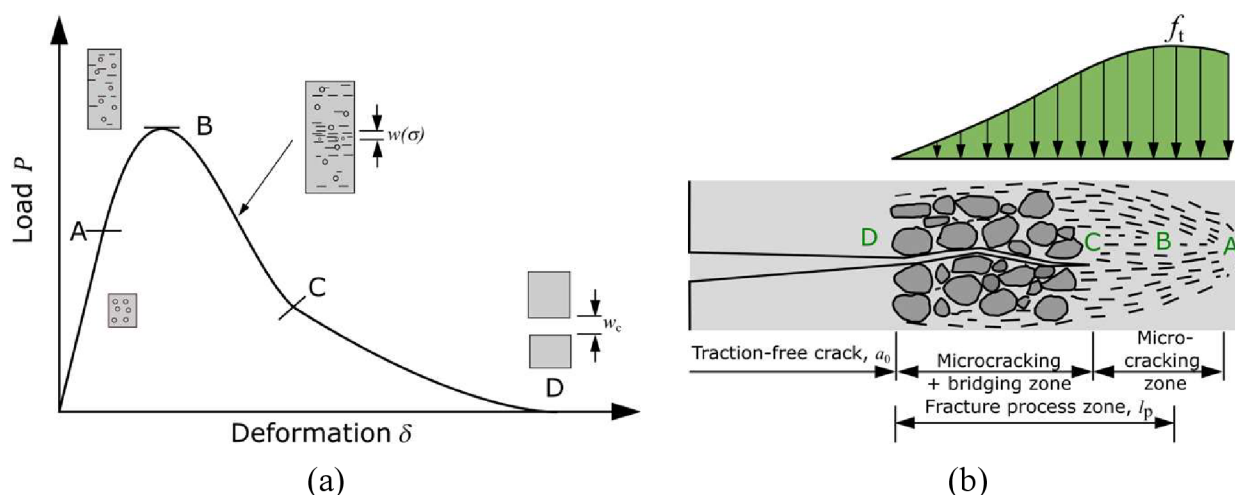
**Figure 5:** Typical $P$-$\delta$ response of a pre-cracked concrete specimen (a), and the fracture process zone ahead of the real traction-free crack (b). Adopted from [49].

This FPZ is known to be property of all quasi-brittle materials, which are mainly heterogenous materials consisting of brittle constituents and inhomogeneities not negligible to the structure's size. These materials include concrete, as the archetypical case, fibre-reinforced concrete, shale and various rocks, fibre-polymer composites, coarse-grained or toughened ceramics, refractories, bone, cartilage, dentine, dental cements, silt, grouted soils, sea ice, consolidated snow, cold asphalt concrete, coal, various printed materials, etc., and all brittle materials on the micrometre scale [50].

Furthermore, the length of this FPZ in concrete structures is not constant, but related to the maximum aggregate size $D_{max}$ a typical value is roughly $12D_{max}$ [51]. This means that, depending on the structural size, the FPZ may encompass the whole cross-section [52]. This influence of the aggregate size on the length of the FPZ was experimentally studied by Mihashi [53] with the acoustic emission (AE) technique.

The development in of the FPZ in concrete is changing over the $P$-$\delta$ process. The concrete material is progressively softening in this zone due to micro-cracking. This can be schematically explained by Figure 5. It is appropriate to highlight significant features of this zone. The linear-elastic behaviour is until the point A is reached. The region between point A and point B exhibits the pre-peak nonlinearity, in which the FPZ is formed. In between the points B and C, the after peak softening is reached as a result of fully formed FPZ and micro-cracking. The tail of softening diagram C-D is on the other hand result of aggregate interlock and other frictional effects. At this stage the macro crack is fully developed.

14

## 1.2  Stress Fields for Mixed mode I/II

The abovementioned LEFM concept derived by Williams uses, in most of the applications, the stress field in the close vicinity of the crack tip described by Williams' expansion (WE) [45]. After receiving solution and some mathematical manipulation the WE can be rewritten into stress tensor form, which accuracy depends on the number of terms used and known stress function. The stress tensor using in Cartesian coordinates for mode I and mode II described by WE have a following form:

$$
\begin{Bmatrix} \sigma_{xx} \\ \sigma_{yy} \\ \sigma_{xy} \end{Bmatrix} = \sum_{n=1}^{\infty} \frac{n}{2} A_n r^{\left(\frac{n}{2}-1\right)} \begin{Bmatrix} \left(2 + \frac{n}{2} + (-1)^n\right) cos\left(\frac{n}{2}-1\right)\theta - \left(\frac{n}{2}-1\right) cos\left(\frac{n}{2}-3\right)\theta \\ \left(2 - \frac{n}{2} - (-1)^n\right) cos\left(\frac{n}{2}-1\right)\theta + \left(\frac{n}{2}-1\right) cos\left(\frac{n}{2}-3\right)\theta \\ \left(\frac{n}{2}-1\right) sin\left(\frac{n}{2}-3\right)\theta - \left(\frac{n}{2}+(-1)^n\right) sin\left(\frac{n}{2}-1\right)\theta \end{Bmatrix}
$$
$$
- \sum_{m=1}^{\infty} \frac{m}{2} B_n r^{\left(\frac{m}{2}-1\right)} \begin{Bmatrix} \left(2 + \frac{m}{2} - (-1)^m\right) sin\left(\frac{m}{2}-1\right)\theta - \left(\frac{m}{2}-1\right) sin\left(\frac{m}{2}-3\right)\theta \\ \left(2 - \frac{m}{2} + (-1)^m\right) sin\left(\frac{m}{2}-1\right)\theta + \left(\frac{m}{2}-1\right) sin\left(\frac{m}{2}-3\right)\theta \\ -\left(\frac{m}{2}-1\right) cos\left(\frac{m}{2}-3\right)\theta + \left(\frac{m}{2}-(-1)^m\right) cos\left(\frac{m}{2}-1\right)\theta \end{Bmatrix},
$$

(1)

where $r$ and $\theta$ are the polar coordinates, $n$, $m$ are the orders of the term in the WE infinite power series, coefficient $A_n$ corresponds to mode I and coefficient $B_m$ corresponds to mode II. The coefficient of the first singular term for $n = 1$, i.e. $A_1$, is related to the stress intensity factor (SIF) for mode I, and the second coefficient $A_2$ corresponds to the distance-independent term called $T$-stress. For mode II the first singular term for $m = 1$, i.e. $B_1$, is related to the SIF for mode II.

These engineering terms can be calculated as follows:

$$ K_I = \sqrt{2\pi} A_1, T = 4A_2, K_{II} = -\sqrt{2\pi} B_1. \tag{2} $$

Using Eq. (2) a stress tensor from Eq. (1) can be rewritten into a simplified two-parameter form:

$$ \sigma_{i,j} = \frac{K_I}{\sqrt{2\pi r}} f_{i,j}^I(\theta) + \frac{K_{II}}{\sqrt{2\pi r}} f_{i,j}^{II}(\theta) + T + O_{i,j}(r,\theta) \tag{3} $$

where $\sigma_{ij}$ represents the stress tensor components, $K_I$, $K_{II}$ are the SIFs for mode I and mode II, respectively.

The $f_{i,j}^I(\theta)$, $f_{i,j}^{II}(\theta)$, are known shape functions for mode I and mode II (with origin at the crack tip; crack faces lie along the ($x$-axis) and $O_{i,j}$ are the higher order (HO) terms. The Cartesian coordinate system formulation for the stress tensor used in Eq. (1) is shown in Figure 6(a), while the same stress tensor in polar coordinates is shown in Figure 6(b).

(a)                                                        (b)
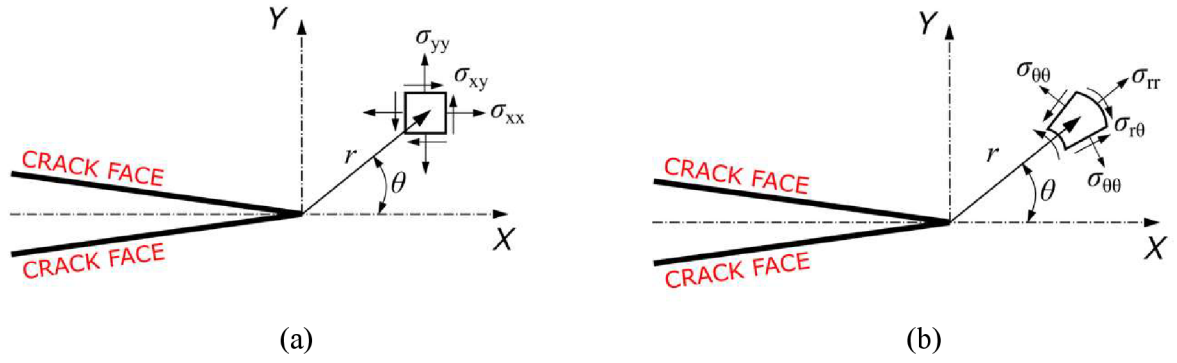
**Figure 6:** Stress tensor components in the Cartesian coordinate system (a) and in the polar coordinate system (b) with the origin at the crack tip.

Further in this thesis, for the description of the stress fields around the crack tip a polar coordinate system is used. For this a stress tensor component using SIFs and $T$-stress can be expressed in following form:

$$\sigma_{\theta\theta} = \frac{K_I}{\sqrt{2\pi r}} cos\left(\frac{\theta}{2}\right)\left[cos^2\left(\frac{\theta}{2}\right)\right] - \frac{K_{II}}{\sqrt{2\pi r}} sin\left(\frac{\theta}{2}\right)\left[3cos^2\left(\frac{\theta}{2}\right)\right] + Tsin^2\theta + O\left(r^{1/2}\right). \qquad (4)$$

As with the stresses, the displacement field for mixed mode I/II load conditions around the crack tip can be expressed using the WE . The displacement in the direction of $x$-axis $u$ is expressed as:

$$u = \sum_{n=0}^{N} \frac{A_n}{2\mu} r^{\frac{n}{2}} \left\{\left(\kappa + \frac{n}{2} + (-1)^n\right) cos\frac{n}{2}\theta - \frac{n}{2} cos\left(\frac{n}{2} - 2\right)\theta\right\}$$

$$+ \sum_{m=0}^{M} \frac{B_m}{2\mu} r^{\frac{m}{2}} \left\{\left(-\kappa - \frac{m}{2} + (-1)^m\right) sin\frac{m}{2}\theta + \frac{m}{2} sin\left(\frac{m}{2} - 2\right)\theta\right\}, \qquad (5)$$

while the displacement in the direction of $y$-axis $v$ is expressed as:

$$v = \sum_{n=0}^{N} \frac{A_n}{2\mu} r^{\frac{n}{2}} \left\{\left(\kappa - \frac{n}{2} - (-1)^n\right) sin\frac{n}{2}\theta - \frac{n}{2} sin\left(\frac{n}{2} - 2\right)\theta\right\}$$

$$+ \sum_{m=0}^{M} \frac{B_m}{2\mu} r^{\frac{m}{2}} \left\{\left(\kappa - \frac{m}{2} + (-1)^m\right) cos\frac{m}{2}\theta + \frac{m}{2} cos\left(\frac{m}{2} - 2\right)\theta\right\}, \qquad (6)$$

where $u$ and $v$ are the displacement vector components in the $x$ and $y$ direction, $\mu$ is the shear modulus, which can be expressed as $E/2(1 + v)$, $\kappa$ is Kolosov's constant for plane strain $3 - 4v$ and for plane stress $(3 - v)/(1 + v)$ conditions, and $E$ and $v$ are the Young's modulus and the Poisson's ratio, respectively.

## 1.3  Mixed Mode I/II Fracture criteria

In the engineering practice the structure or its components are very often loaded with multiple types of loads which produce the mixed mode I/II fracture. Knowledge of

16

the direction of the crack initiation can help to extend the structure's life and reduce structure's sudden failures. S

Usually the mixed mode I/II fracture analysis is done by employing various fracture criteria. Traditional criteria are e.g. maximum tangential stress (MTS) criterion postulated by Erdogan and Sih in 1963 [54] and strain energy density (SED) criterion postulated by Sih in 1974 [55, 56]. Both criteria use in the mixed mode I/II fracture analysis only SIFs for mode I and mode II. The recent development of fracture analysis of mixed mode I/II loading conditions lead to postulate advanced fracture criteria e.g. generalized strain energy density (GSED) criterion [57, 58] and generalized maximum tangential stress (GMTS) criterion [59, 60]. These recent fracture criteria are using SIFs as well as the traditional ones together with additional parameters. These parameters are the $T$-stress (i.e. the second term of the WE) or more WE terms and the critical distance $r_C$. Employment of additional parameters leads to more computationally demanded procedures, which are mainly solved numerically.

### 1.3.1 Generalised Maximum Tangential Criterion

The GMTS criterion is extension of the traditional MTS criterion. The GMTS, uses the tangential stress $\sigma_{\theta\theta}$ as presented in Eq. (4) on p. 16. The $\sigma_{\theta\theta}$ is expressed by using first two engineering terms presented in Eq. (2) on p. 15 i.e. $K_I$ and $T$ for mode I and $K_{II}$ for mode II.

The maximum value is found by search for function maximum and by complying to the conditions, then crack initiation direction $\theta_0$ can be obtained from conditions when:

$$\frac{\partial \sigma_{\theta\theta}}{\partial \theta}|_{\theta=\theta_0} = 0 \text{ and } \frac{\partial^2 \sigma_{\theta\theta}}{\partial^2\theta} < 0. \tag{7}$$

This modifies Eq. (4) on p. 16 to following form of MTS criterion:

$$[K_I sin\theta_0 + K_{II}(3cos\theta_0 - 1)] = 0 \tag{8}$$

or in GMTS form:

$$[K_I sin\theta_0 + K_{II}(3cos\theta_0 - 1)] - \frac{16T}{3}\sqrt{2\pi r_c}cos\theta_0 sin\frac{\theta_0}{2} = 0. \tag{9}$$

The main difference between Eq. (8) and Eq. (9) is that the crack initiation angle $\theta_0$ of the maximum tangential stress $\sigma_{\theta\theta}$ for any combination of modes I and II depends on $K_I$, $K_{II}$, $T$ and on the critical distance $r_C$. Please note, if the critical distance $r_C = 0$, the GMTS expression simplified itself to MTS expression as presented in Eq. (8). The angle $\theta_0$ determined from Eq. (9) is then used to predict the direction of the mixed mode I/II fracture.
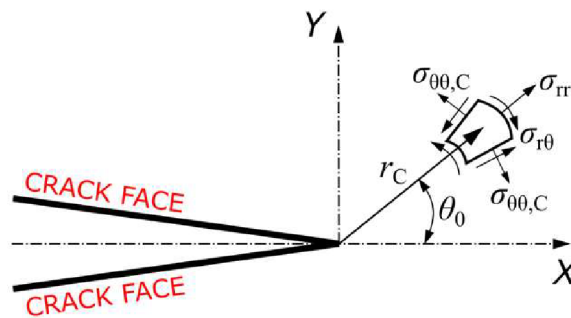
**Figure 7:** Stress tensor in polar coordinates with a critical distance $r_C$, onset of fracture $\theta_0$ and critical tangential stress $\sigma_{\theta\theta,C}$ with the origin at the crack tip.

According to GMTS criterion for mixed mode I/II, the brittle fracture occurs radially from the crack in the direction of the maximum tangential stress $\theta_0$. The crack initiate when along the $\theta_0$ and critical distance $r_C$ the maximum tangential stress $\sigma_{\theta\theta}$ reaches its critical value $\sigma_{\theta\theta,C}$ (See Figure 7). The brittle fracture occurs when $K_I = K_{IC}$, $K_{II} = 0$. and $\theta_0 = 0°$, this assumption simplifies Eq. (4) on p. 16 to:

$$\sqrt{2\pi r_C}\,\sigma_{\theta\theta,C} = K_{IC},\tag{10}$$

where $K_{IC}$ is the fracture toughness for mode I.

The brittle fracture can be obtained by substituting the fracture toughness $K_{IC}$ and found crack initiation direction $\theta_0$ into Eq. (4). This will lead to:

$$K_{Ic} = \cos\frac{\theta_0}{2}\left[K_I \cos^2\frac{\theta_0}{2} - \frac{3}{2}K_{II}\sin\theta_0\right] + \sqrt{2\pi r_c}\,T\sin^2\theta_0.\tag{11}$$

Such Eq. (11) can be used for the calculation of fracture initiation for pure mode I, pure mode II and mixed mode I/II.

### 1.3.2  Critical Distance

It is recognized that plastic deformation will occur at the crack tip or in its close vicinity as a result of the high stresses that are generated by the sharp stress concentration. To estimate the extent of this plastic deformation, Irwin equated the yield strength to the *Y*-direction stress along the *X*-axis and solved it for the radius. The radius value determined was the distance along the *X*-axis where the stress perpendicular to the crack direction would equal the yield strength; thus, Irwin [61] found that the extent of plastic deformation. This extent of the plastic zone is now commonly referred as critical distance $r_C$. The fundamental approach to acquire the values of material's critical distance can be evaluated by substituting material's fracture toughness $K_{IC}$ into tangential stress $\sigma_{\theta\theta}$ from Eq. (4) on p. 16 or its critical value $\sigma_{\theta\theta,C}$ from

Eq. (10) on p. 18 and considering various boundary conditions, this will lead to following formulas:

$$r_c = \frac{1}{2\pi}\left(\frac{K_{IC}}{\sigma_t}\right)^2 - \text{plane stress,} \tag{12}$$

$$r_c = \frac{1}{6\pi}\left(\frac{K_{IC}}{\sigma_t}\right)^2 - \text{plane strain.} \tag{13}$$

In Eqs. (12) and (13) $K_{\text{IC}}$ is the fracture toughness for mode I and $\sigma_t$ is the tensile strength or sometimes referred as $f_t$ in application to concrete materials.

# 2 Experimental Details

## 2.1 Test specimens

The Brazilian disc (BD) is widely used to determinate the indirect or transverse tensile strength $f_t$ of rocks [36] (see Figure 8(a)). While the Brazilian Disc with a Central Notch (BDCN) was selected as a main geometry to investigate the mixed mode I/II fracture. This mixed mode I/II loading is achieved by inclining the initial notch to the loading point by the angle $\alpha$ (see Figure 8(b). The dimensions and typical boundary conditions for both tests are shown Figure 8.



(a)                                        (b)
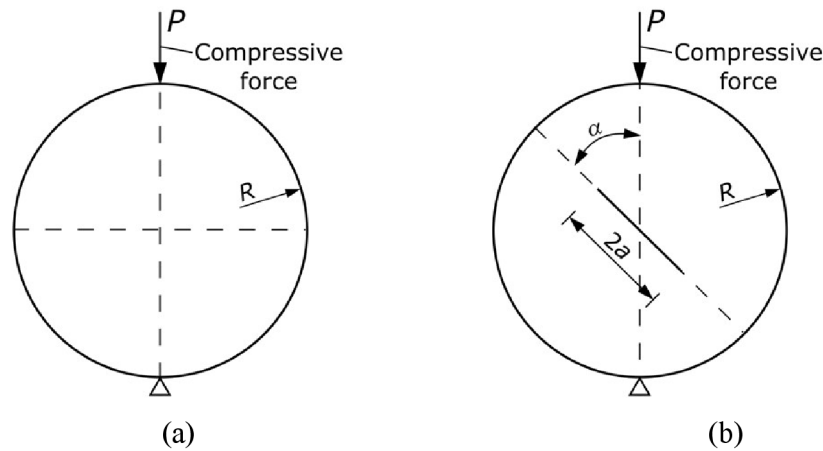
**Figure 8:** Dimensions and boundary conditions of – (a) Brazilian disc specimen and (b) Brazilian disc with a central notch specimen.

The indirect tensile strength $f_t$ can be evaluated for the BD specimen by the following equation:

$$f_t = \frac{P}{\pi RB}, \tag{14}$$

where $P$ is the applied compressive load, $R$ is the disc's radius and $B$ is the specimen's thickness.

The BD's failure occurs in centre of the disc in the location of the maximum tensile stress. Measured indirect tensile strength $f_t$ is used to determinate material's critical

distance $r_C$ as it is evaluated from circular geometry which reduce the error produced by different geometries.

Both BD and BDCN specimens are prepared by cuts of the cylindrical samples. The cylindrical sample can be obtained from core drill (real structure prior to renovation) or from mixture cast to moulds (new mixture development). In this study the specimens have been made from moulded samples with dimension of 150 × 300 mm (height × diameter). Actual, experimental setup for the BDCN specimen is showed in Figure 9.



(a)                                                    (b)
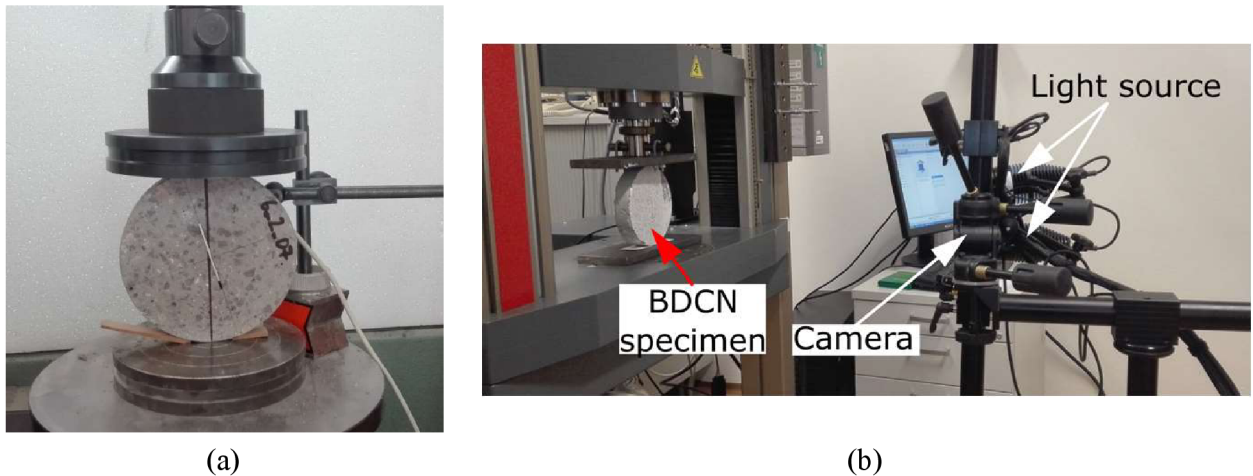
**Figure 9:** Experimental set-up of BDCN specimen ($a/R = 0.4$ $\alpha = 20°$) (a) and (b) the DIC measurement setup.

The notch in the BDCN specimen has length of $2a$ and the relative notch length ratio is then expressed as $a/R$ and thus the notched specimen is used in the evaluation of FMPs of concrete materials.

Further in the analysis of the mixed mode I/II fracture resistance the SIFs will be determined on the BDCN geometry. The SIFs for mode I and mode II are calculated using Eqs. (15) and (16) according to the handbook by Tada & Paris [62] and by the literature Ayatollahi [60] and by Seitl et al [63].

$$K_I = \frac{P\sqrt{a}}{RB\sqrt{\pi}} \frac{1}{\sqrt{1 - \dfrac{a}{R}}} Y_I(a/R, \alpha), \tag{15}$$

$$K_{II} = \frac{P\sqrt{a}}{RB\sqrt{\pi}} \frac{1}{\sqrt{1 - \dfrac{a}{R}}} Y_{II}(a/R, \alpha), \tag{16}$$

where $P$ is the applied compressive load, $R$ is the specimen radius, $a$ is the crack length, $\alpha$ is the notch inclination angle, $B$ is the thickness of the specimen and $Y_I$ and $Y_{II}$ are the shape functions for mode I and mode II, respectively.

The mixed mode I/II fracture resistance is usually expressed in the relative coordinates for mode I as ratio of $K_I/K_{IC}$ and for mode II as ratio of $K_{II}/K_{IC}$.

The fracture resistance is then expressed by substituting these assumptions to the Eq. (11) on p. 18. The fracture resistance curve for mode I is then obtained from:

$$\frac{K_{IC}}{K_I} = cos\frac{\theta_0}{2}\left[cos^2\frac{\theta_0}{2} - \frac{3}{2}\frac{K_{II}}{K_I}sin\theta_0\right] + \sqrt{2\pi r_c}\frac{T}{K_I}sin^2\theta_0, \qquad (17)$$

and for mode II:

$$\frac{K_{IC}}{K_{II}} = cos\frac{\theta_0}{2}\left[\frac{K_I}{K_{II}}cos^2\frac{\theta_0}{2} - \frac{3}{2}sin\theta_0\right] + \sqrt{2\pi r_c}\frac{T}{K_{II}}sin^2\theta_0, \qquad (18)$$

Both Eq. (17) and Eq. (18) show noticeable dependency of whole GMTS criterion on the second term of the WE and on the critical distance $r_C$. Thus, the estimation of proper value of the critical distance $r_C$ in this case is crucial.

In order to study the influence of the aggressive environment on the mixed mode I/II, the prepared BD and BDCN samples were stored in plastic containers filled with water and sodium chloride solution. The samples were stored in such conditions for 30 days. The containers are shown in Figure 10.



**Figure 10:** Prepared BD and BDCN specimens stored in plastic containers filled with water and chloride solution in a laboratory room with constant room temperature.

## 2.2  Materials

Hereunder, the used concrete mixtures are presented in form of measured mechanical characteristics. The total number of used mixtures for this experimental campaign is 5 i.e., C 50/60, HSC, HPC - batch A, AAC and HPC- batch B. The mixture composition was in direct cooperation with the concrete precast plant at ŽPSV s.r.o. company. Presented mixtures are used in the prefabrication of the concrete structural ele-

ments e.g. bridge beams, floor panels and the railway sleepers. The intent of investigation of more than one mixture is to improve its mechanical and mainly fracture mechanical properties, while reducing the cement content. The measured material's mechanical properties are according to European standards.

**Table 1:** Mechanical properties of used concrete mixturesat 28 days age.

|  | C 50/60 | HSC | HPC_A | AAC | HPC_B |
|---|---|---|---|---|---|
| Compressive cube strength $f_{c,cube}$ [MPa] | 85.8 | 65.2 | 51.1 | 62.3 | 60.8 |
| Compressive cylindrical strength $f_{c,cyl}$ [MPa] | 72.8 | 106.2 | 100.5 | 48 | 102.0 |
| Indirect tensile strength $f_t$ [MPa] | 5.52 | 7.4 | 5.4 | 3.4 | 6.2 |
| Young's Modulus $E$ [GPa] | 38.3 | 41.3 | 42.1 | 26.3 | 28.7 |
| Young's modulus – cylinder $E_{cyl}$ [GPa] | 39.2 | - | 40.6 | 29.6 | 39.5 |
| Bulk density $\rho$ [kg/m$^3$] | 2390 | 2350 | 2342 | 2210 | 2395 |

## 3  Numerical Model

In order to assess the relevance of the BDCN test, a parametric study of a BDCN was performed using the FEM software Abaqus [64] with concrete damage plasticity material model. For this, 2D plane stress model was created with a radius of $R = 75$ mm corresponding to the disc's size in [65], and an initial notch length $2a = 60$ mm corresponding to a relative crack length $a/R = 0.4$, a notch thickness $t$ of 2 mm and inclination notch angles $\alpha$ of 0°, 5° 10°, 15°, 20° and 25.2°. The initial notch angle $\alpha_n$ was selected to investigate the tensile mode I fracture i.e. $\alpha = 0°$, the mixed mode I/II fracture for angle $\alpha$, which varies from 5° to 20°. The pure shear mode II fracture should be present when $\alpha = 25.2°$ [65].

The LEFM model was loaded by the force $P$ of 100 N in order to obtain geometry functions for mode I $Y_I$ and for mode II $Y_{II}$ and to have values of $T$-stress for various $a/R$ ratios.

The numerical study was performed with a displacement-controlled loading applied at the top edge of the BDCN, while the bottom edge was considered a rigid support. The total induced vertical displacement was $u_y = -0.1$ mm ($u_x = 0$ mm) over the pseudo time step (static analysis). Adequate boundary conditions were added to prevent rigid body translations and rotations (See Figure 11).

(a)
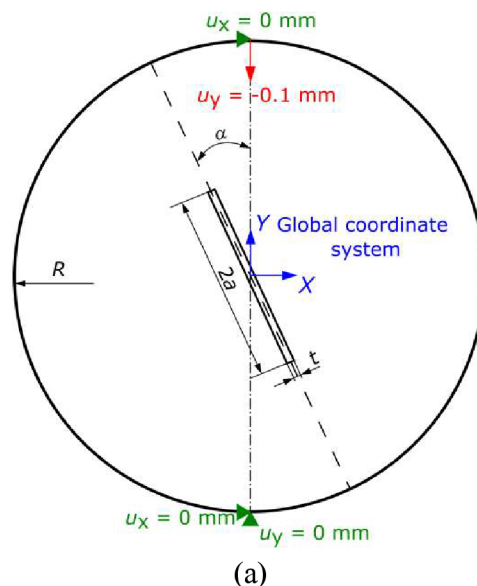
**Figure 11:** Geometry and boundary conditions (a) and flattened edge of BDCN model (b).

## 3.1  Numerical results

To evaluate the values of geometry function $Y_I$ and $Y_{II}$ a numerical model, the LEFM was used to calculate SIFs for mode I and mode II for various notch lengths $a/R$ and initial notch inclination angle $\alpha$. The relative notch lengths were selected as 0.2, 0.267, 0.3, 0.5, and 0.6 and values of notch inclination angle $\alpha$ were <0° - 45°>. The evaluated geometry functions $Y_I$ and $Y_{II}$ for various $a/R$ ratios are presented in Figure 12.



(a)                                                    (b)
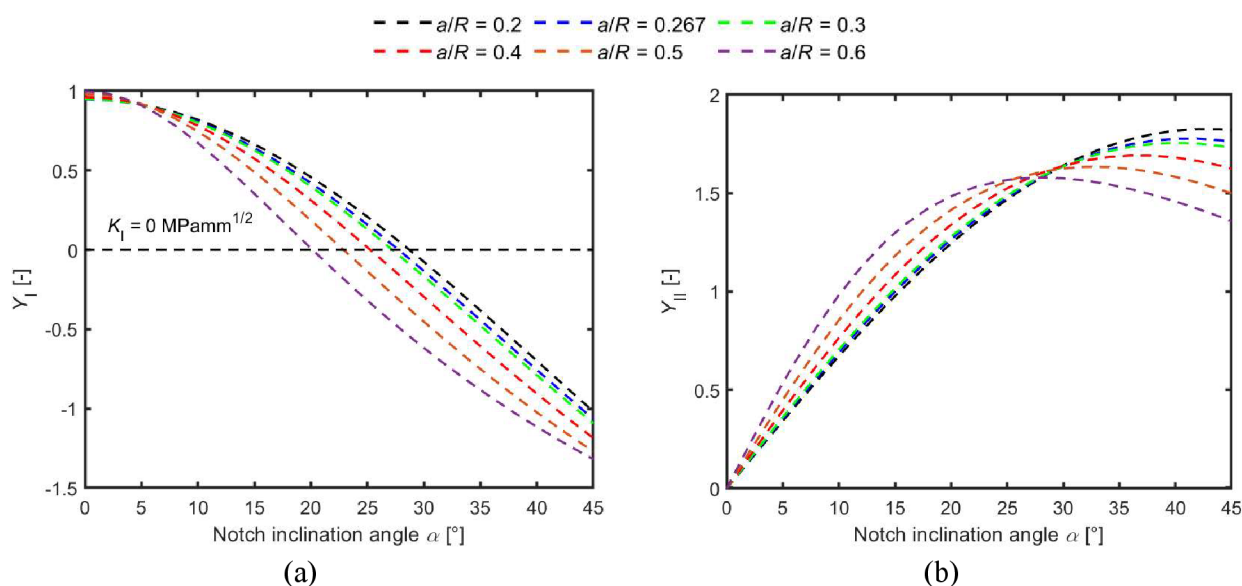
**Figure 12:** Comparison of geometry function values for various $a/R$ ratios - (a) for mode I $Y_I$ and (b) for mode II $Y_{II}$.

The negative values of geometry functions $Y_I$, as observed in Figure 12, is related to the interface free crack faces, which results into overlapping the crack faces in the numerical solution. In practice, the negative value of $Y_I$ and $K_I$ would arrest the crack

initiation. Similarly to SIFs, $T$-stress values can be generated by FEM model. The numerically calculated $T$-stress values for various $a/R$ ratios are shown in Figure 13.
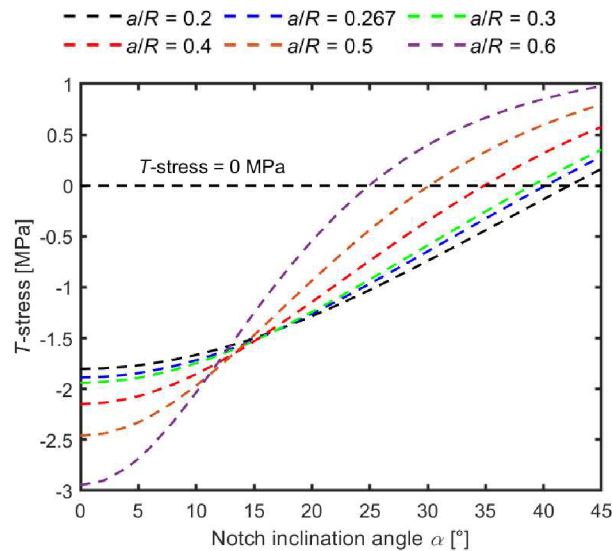


**Figure 13:** Comparison the numerical generated $T$-stress values for various relative notch length $a/R$ corresponding to load $P = 100$ N.

Wide range of notch inclination angle $\alpha$ was chosen to demonstrate the fact that the pure mode II is present for different angle $\alpha$ for each studied $a/R$ ratio. Similarly to this, the values of the $T$-stress are presented in order to show for which angle $\alpha$ is $T$-stress equal to 0. The detailed values of notch inclination angles $\alpha$ for which $Y_I = 0$ ($\alpha_{Y_I=0}$) and $T$-stress = 0 ($\alpha_{T=0}$) are showed in Table 2.

**Table 2:** Comparison of angle $\alpha$ for which $Y_I = 0$ and $T$-stress = 0 for various $a/R$ ratios.

| $a/R$ [-] | $\alpha_{Y_I=0}$ [°] | $Y_I$ [-] | $\alpha_{T=0}$ [°] | $T$-stress [MPa] |
|---|---|---|---|---|
| 0.2 | 29 | 0.05 | 42 | -0.013 |
| 0.267 | 27.7 | 0.003 | 40 | -0.001 |
| 0.3 | 28 | 0.201 | 38 | -0.061 |
| 0.4 | 25.2 | 0.002 | 34 | -0.058 |
| 0.5 | 22 | 0.374 | 26 | -0.008 |
| 0.6 | 20 | 0.078 | 25 | 0.008 |

The non-linear numerical analysis provides overall comparison of the maximum reaction loads is presented in Figure 14 (a), where the difference between average values of numerical and experimental data is limited to 16% for angles $\alpha$ higher than 25°. Nevertheless, the numerical and experimental values of $P_{max}$ show similar trend. This can be seen in the Figure 14(b), where the linear function based on the least square method was used on the average values.
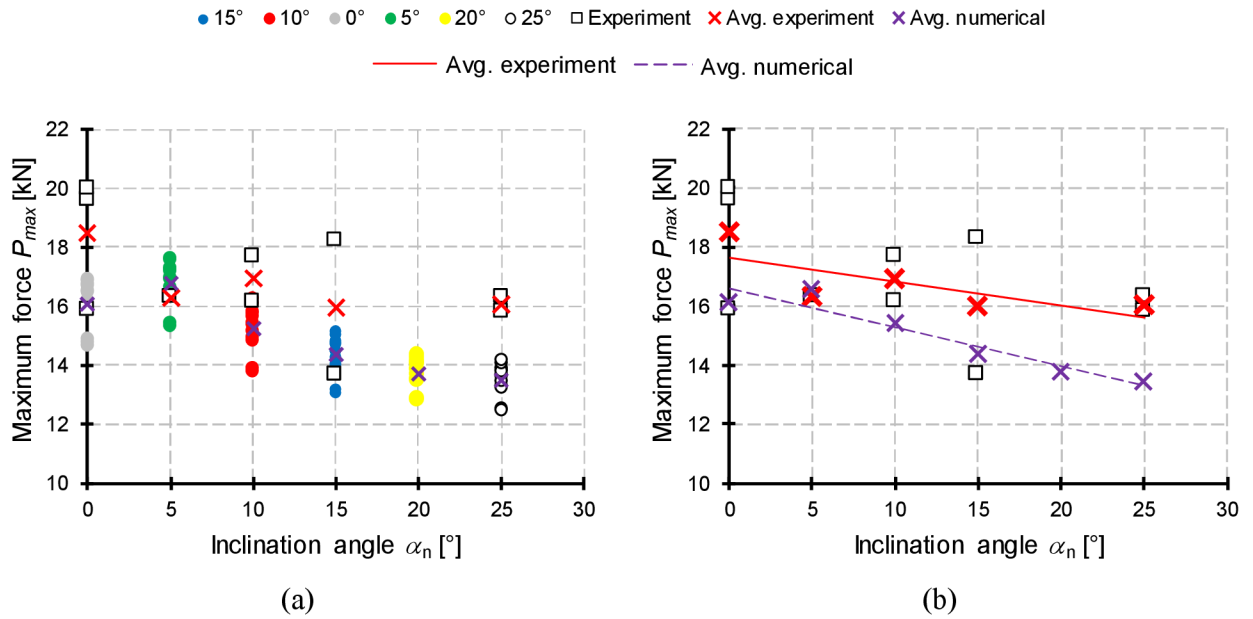
**Figure 14:** Comparison of maximum calculated forces $P_{\max}$ with experimentally measured fracture forces $P_C$ from Seit et al. [65] i.e. on the C 50/60 material.

# 4 Experimental Results

## 4.1 Fracture Toughness

The pure mode I is present for both relative ratios $a/R$ of 0.267 and 0.4 for notch inclination angle $\alpha = 0°$. On the other hand, the pure mode II is present at different inclination angle for each ratio $a/R$. Thus, the mode II fracture toughness was determined for angle $\alpha = 27.7°$ for the ratio $a/R = 0.267$ and for angle $\alpha = 25.2°$ for the ratio $a/R = 0.4$. Determined values of fracture toughness for mode I $K_{IC}$ for each studied material are presented in Table 3, while values of fracture toughness for mode II $K_{IIC}$ are showed in Table 4.

**Table 3:** Comparison of evaluated fracture toughness $K_{IC}$ for mode I on the BDCN geometry for various relative notch lengths.

| Material | $a/R = 0.267$ $K_{IC}$ [MPam$^{1/2}$] | $a/R = 0.4$ $K_{IC}$ [MPam$^{1/2}$] |
|---|---|---|
| C 50/60 | 0.668 | 0.972 |
| High-strength concrete | 1.064 | 1.821 |
| High-performance concrete – Batch A | 0.790 | 0.8423 |
| Alkali activated concrete | 0.551 | 0.584 |
| HPC - Batch B- Cl$^-$ free | - | 0.919 |
| HPC - Batch B - Cl$^-$ saturated | - | 0.782 |

**Table 4:** Comparison of evaluated fracture toughness $K_{IIC}$ for mode II on the BDCN geometry for various relative notch lengths.

| Material | $a/R = 0.267$ $K_{IIC}$ [MPam$^{1/2}$] | $a/R = 0.4$ $K_{IIC}$ [MPam$^{1/2}$] |
|---|---|---|
| C 50/60 | 0.974 | 1.329 |
| High-strength concrete | 1.835 | 2.290 |
| High-performance concrete – Batch A | 1.229 | 1.182 |
| Alkali activated concrete | 0.730 | 1.084 |
| HPC – Batch B - Cl⁻ free | - | 1.105 |
| HPC – Batch B - Cl⁻ saturated | - | 1.073 |

From values presented in Table 3 and Table 4 it can be observed, that the values of both fracture toughness vary heavily. This difference is caused by geometry and by material itself, which vary in the mixture composition. Clear increase by at least 15% of both values $K_{IC}$ and $K_{IIC}$ for the mixtures categorized as HPC or HSC can be observed, if compared to C 50/60 material. The highest difference shows HSC mixture with almost 55 % increase of the $K_{IC}$ value and by 60% increase of the $K_{IIC}$ value. On the other hand, if C 50/60 is compared to AAC material a decrease by 40% of $K_{IC}$ and by 25% of $K_{IIC}$ can be observed.

Both changes are mainly related to the value of indirect tensile strength $f_t$, which depends on the bond between the aggregate and matrix. Decrease of $K_{IC}$ value in case of AAC material is due to overall lower mechanical performance (compressive strength, tensile strength) of the material, which results to an earlier crack initiation and specimen failure. On the other hand, decrease in in case of chloride environment is related to the possible formation of the Friedel's salt as the Portland cement blend contains Metakaolin, which increase the chance of the Friedel's salt formation.

### 4.2 Critical Distance

In further evaluation of the mixed mode I/II fracture resistance, the critical distance $r_C$ plays key role and varies for each material. Critical distance $r_C$ depends on the fracture toughness $K_{IC}$ for mode I and on the tensile strength $f_t$, simultaneously it is parameter which governs the fracture resistance under the mixed mode I/II evaluated by GMTS criterion.

As above-mentioned approach to calculate the critical distances $r_C$ offers two variants for its calculation as showed in Eq. (12) and in Eq. (13) on p. 19. The calculated $r_C$ for all investigated concrete mixtures and relative notch ratios $a/R$ are presented in Table 5.

**Table 5:** Comparison of calculated critical distance $r_C$ for various studied concrete materials.

| Material | Plane stress $r_C$ [mm] | | Plane strain $r_C$ [mm] | |
|---|---|---|---|---|
| | $a/R = 0.267$ | $a/R = 0.4$ | $a/R = 0.267$ | $a/R = 0.4$ |
| C 50/60 | 2.336 | 4.945 | 0.779 | 1.648 |
| HSC 7.6. | 1.607 | 4.711 | 0.536 | 1.570 |
| HPC 31.5. | 2.402 | 2.730 | 0.801 | 0.91 |
| ACC | 4.856 | 5.459 | 1.619 | 1.820 |
| HPC – Cl⁻-free | - | 3.975 | - | 1.325 |
| HPC – Cl⁻-saturated | - | 2.873 | - | 0.958 |

From Table 4 a similar observation as in the case of the fracture toughness $K_{IC}$ can be made i.e. the critical distance The discussion is about the selection of the critical distance $r_C$ from the crack tip and its influence on the shape and size of the fracture resistance curve.
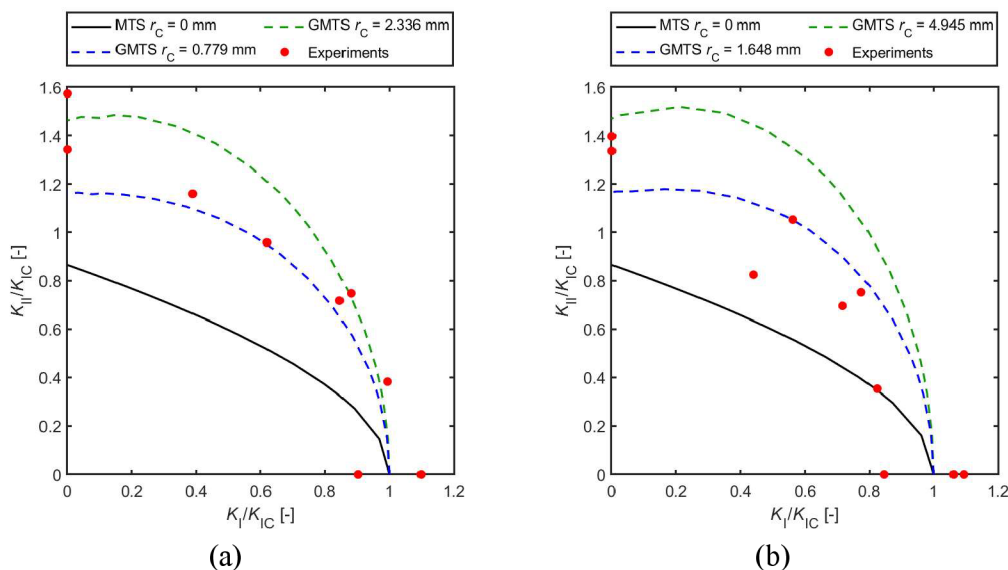
## 4.3  Mixed Mode I/II Fracture Resistance

To evaluate the fracture resistance under the mixed mode I/II the GMTS criterion was used. The mixed mode fracture resistance of each studied concrete mixture is present in form of the fracture resistance curve, which was calculated from Eqs. (12) and (13)on p.19 for various critical distances. Such curves are presented in relative and absolute values.

Generally, the mixed mode I/II fracture resistance is presented in relative coordinates, i.e. $K_I/K_{IC}$ as for the $x$-axis and $K_{II}/K_{IC}$ as for the $y$-axis. This provides great illustration of how accurate the theoretical prediction by the fracture criterion is. Subsequently, the goodness of fracture resistance predicted by fracture criteria was estimated by the root mean squared error (RSME) to give explicit conclusions.
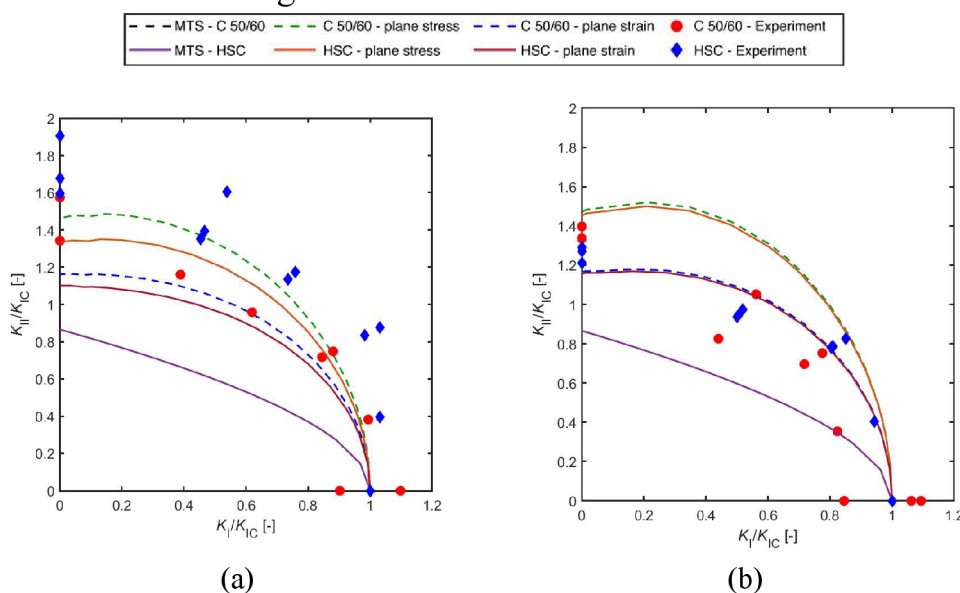
## 4.4  Fracture Resistance Curves

The BDCN specimen made of C 50/60 material were used in preliminary experiments for first try out of such experimental setup. Experiments were performed with the BDCN possessing the notch of relative crack ratio $a/R$ of 0.267 and $a/R$ of 0.4.

Mixed mode I/II fracture resistance for C 50/60 evaluated by using the MTS (Eq. (8) on p. 17) and GMTS criterion (Eq. (9) and  (8) on p. 17) with the values of fracture toughness from Table 3 for $a/R$ of 267 and from Table 4 for $a/R$ of 0.4. Subsequently, values of critical distance as presented in Table 5 were used as input parameters for the fracture criteria. The estimated fracture resistance curves in relative coordinates, i.e. $K_I/K_{IC}$ and $K_{II}/K_{IC}$ are shown in Figure 15.

**Figure 15:** Mixed mode I/II fracture resistance of C 50/60 material relative notch ratio (a) – $a/R = 0.267$ and (b) – $a/R = 0.4$.

If the fracture resistance curves calculated by GMTS criterion are compared in the relative coordinates, the difference between each mixture is virtually low. The evaluated fracture resistance curves via GMTS criterion for the HSC mixtures in relative coordinates are showed in Figure 16.



**Figure 16:** Comparison of the fracture resistance curves between C 50/60 and HPC material in relative coordinates (a) – $a/R = 0.267$ and (b) – $a/R = 0.4$.

## 4.5    Mixture Comparison

Studied mixtures are compared by means of the value of The calculate RSME values for relative notch ratio $a/R$ of 0.267 are presented in Table 6 and for relative notch ratio $a/R$ of 0.4 are presented in Table 7.

**Table 6:** Comparison of RSME values for the fracture criteria for various materials for ratio $a/R$ of 0.267.

| Material | C 50/60 | HSC | HPC | AAC |
|---|---|---|---|---|
| RSME – MTS [-] | 0.7349 | 0.5865 | 0.6760 | 0.7451 |
| RSME – GMTS – plane stress [-] | 0.9384 | 0.8608 | 0.9615 | 0.8112 |
| RSME – GMTS – plane strain [-] | 0.9322 | 0.7522 | 0.8732 | 0.9679 |

**Table 7:** Comparison of RSME values for the fracture criteria for various materials for ratio $a/R$ of 0.4.

| Material | C 50/60 | HSC | HPC | AAC |
|---|---|---|---|---|
| RSME – MTS [-] | 0.8132 | 0.8064 | 0.7120 | 0.8132 |
| RSME – GMTS – plane stress [-] | 0.8845 | 0.8973 | 0.9428 | 0.8845 |
| RSME – GMTS – plane strain [-] | 0.9155 | 0.9577 | 0.8725 | 0.9155 |

From both Table 6 and Table 7 can be seen that the traditional fracture criterion MTS predicts mixed mode I/II failure inaccurately with almost 40 % of difference.

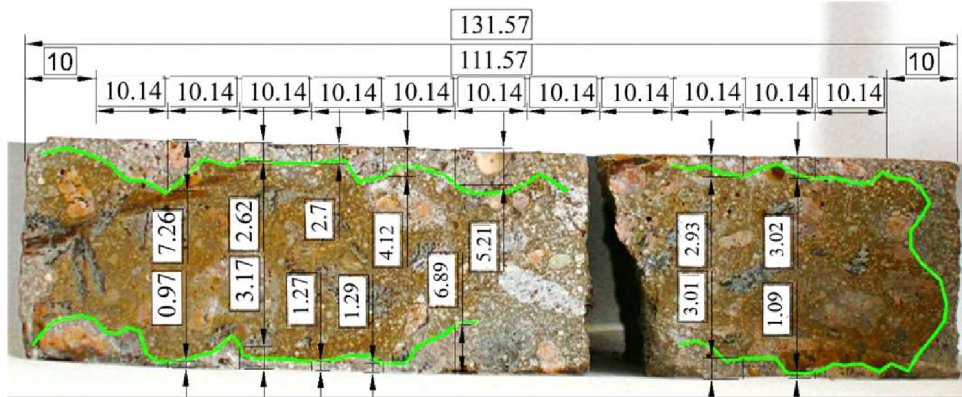## 4.6    Chloride Penetration Depth

The evaluation of the influence of the chloride penetration of the concrete specimen, was investigated whether the weakened cross-section had an effect on the fracture properties. For this purpose, a chloride penetration depth was measured by the afore-mentioned colorimetric method. The average values of the measured penetration depth are shown in Table 8.

**Table 8:** Measured chloride penetration depth.

| Specimen | Penetration depth from the bottom [mm] | Penetration depth from the top [mm] | Mean value of penetration depth [mm] |
|---|---|---|---|
| HPC_37 | 4.79 | 3.11 | 3.95 |
| HPC_38 | 6.45 | 5.72 | 6.09 |
| HPC_39 | 3 | 5.29 | 4.15 |
| Mean value | 4.74 | 4.71 | 4.73 |

Based on the results, one can notice that the specimens were affected by chloride ions approximately 4.73 mm from both the top and the bottom.

The measurement of the chloride penetration depth was conducted by the $AgNO_3$ colorimetric method as described in [66]. After the splitting tests, the chloride-contaminated specimens were sprayed with the $AgNO_3$ solution. The measurement of chloride penetration depths is presented in Figure 17, where the un-penetrated ligament is highlighted with a green line, and the specimen is divided into regular sections.

**Figure 17:** Measured chloride penetration depth by colorimetric method on one of the specimens.

It is necessary to distinguish between the values of fracture toughness $K_{IC}$ measured for the different Cl⁻ environments. Thus, $K_{IC}$ is used for the values of fracture toughness experimentally measured on the Cl⁻-free samples, and $K_{IC}^{Cl^-}$ is used for the values of fracture toughness experimentally measured on the specimens saturated with Cl⁻. The experimental results presented in Figure 18.
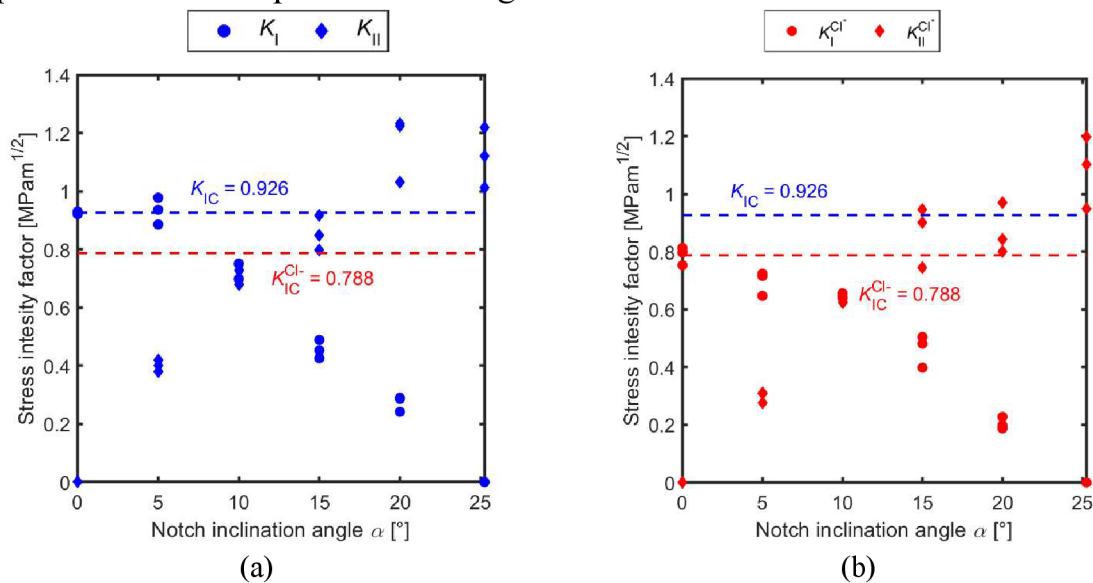


**Figure 18:** Comparison of the evaluated SIF values for various environmental conditions with highlighted values of fracture toughness $K_{IC}$ and $\boldsymbol{K_{IC}^{Cl^-}}$, respectively - (a) Cl⁻-free samples and (b) Cl⁻-saturated samples.

The measured values of the fracture toughness of the HPC concrete mixture exposed to different environments are $K_{IC}$ of 0.926 MPam$^{1/2}$ and $K_{IC}^{Cl^-}$ of 0.788 MPam$^{1/2}$, respectively. This difference seems to be linked to the fact that the Cl⁻ ions penetrate the disc's body not only from both the top and the bottom surface, as in the case of the samples used for the indirect tensile strength measurement, but also Cl⁻ ions can penetrate from the notch, which creates another surface exposed to the Cl⁻ environment.

This leads to a lower value of fracture toughness $K_{IC}^{Cl^-}$, as the crack initiates from the notch end. The calculated values of critical distance $r_C$ for both studied cases of environment aggressivity are presented in Table 9.

**Table 9:** Calculated values of critical distance $r_C$ for both studied cases of Cl⁻-free and Cl⁻-saturated environment aggressivity, respectively.

| Fracture toughness [MPam$^{1/2}$] | $r_C$ [mm] - plane strain | $r_C$ [mm] - plane stress |
|---|---|---|
| $K_{IC} = 0.926$ | 1.344 | 4.033 |
| $K_{IC}^{Cl^-} = 0.788$ | 0.972 | 2.917 |

The calculated critical distances for the case of the Cl⁻-saturated specimens show again a lower value by approx. 30%, which results in an earlier crack initiation and a lower value of fracture toughness $K_{IC}$. According to the GMTS criterion, the onset of a fracture begins when the critical value of tangential stress $\sigma_{\theta\theta,C}$ is reached. In the case of the Cl⁻-saturated samples, the value of $\sigma_{\theta\theta,C}$ is reached in the closer distance from the crack tip, which results in an earlier failure. The comparison of fracture resistance curves for both Cl⁻ free and Cl⁻ saturated cases is presented in Figure 19.
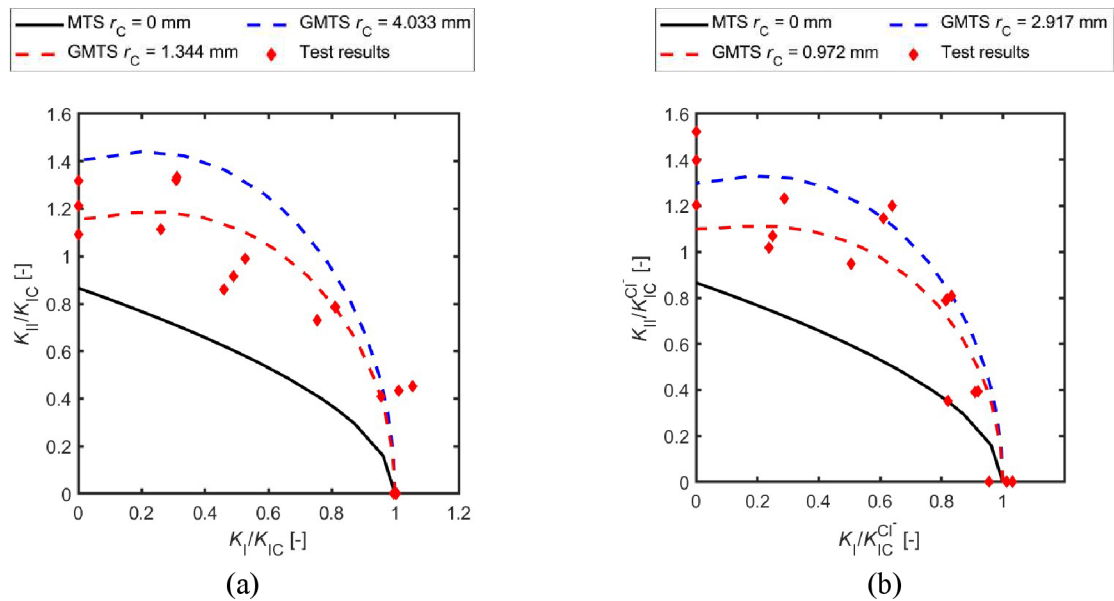


**Figure 19:** Comparison of evaluated fracture resistance curve under the mixed mode I/II loading conditions - (a) chloride Cl⁻-free samples and (b) chloride Cl⁻-saturated samples.

This influence of various levels of the environment aggressivity is more observable, if the fracture resistance curves are plotted in absolute values, i.e. plotted as $K_{II}$ against $K_I$ instead of the ratio of $K_I/K_{IC}$ and $K_{II}/K_{IC}$, respectively. The mixed mode I/II fracture resistance curves with various levels of environment aggressivity are shown for plane stress in Figure 20(a) and for plane strain in Figure 20(b).
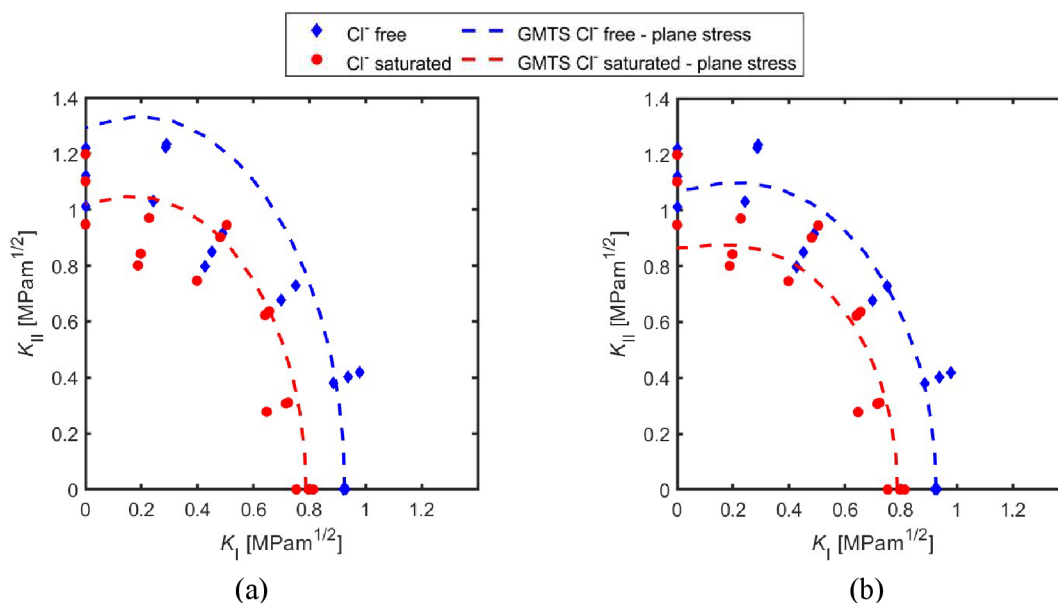
**Figure 20:** Fracture resistance under mixed mode I/II expressed in absolute values of stress intensity factors for mode I and mode II – (a) plane stress and (b) plane strain.

The fracture resistance curves presented in Figure 20 again show a clear influence of the chloride aggressivity on the fracture resistance under the mixed mode I/II load. This difference for both studied cases of the aggressive environment is again about 15%. Consequently, this influence of the chloride penetration on the fracture resistance under mixed mode I/II should be taken into account, as it can lower the fracture load, for which a crack can initiate in a real structure. Moreover, this result has a major influence as it was experimentally proven before, that if HPC mixture has some content of metakaolin, it improves the mixture's resistance to chloride penetration [67].

# Conclusion

The aim of this research was to study the crack initiation under the mixed-mode I/II conditions of various concrete materials used in building practice. The measured fracture mechanical properties and fracture resistance under the mixed-mode I/II of commonly used C 50/60 concrete material were compared to newly developed high-strength, high performance and alkali-activated concrete materials. The mixed mode I/II crack initiation problem was analysed numerically and experimentally on the concrete Brazilian disc with central notch (BDCN) specimen.

The numerical part, focused on the evaluation of the geometry functions of the BDCN geometry Furthermore, the crack initiation and propagation in the BDCN specimen was analysed by the means of the non-linear analysis by employing the concrete damage plasticity material model.

In experimental part, the focus was placed to evaluate the value of material's fracture toughness $K_{IC}$ and the critical distance $r_C$ as they serve as an input parameters to the generalised maximum tangential stress (GMTS) fracture criterion. Furthermore, the influence of the aggressive environment on the values of $K_{IC}$, $r_C$ and the shape of the fracture resistance curve was study on chloride saturated specimens. Experimental Outcome

Experimental results proved that the each mixture shows different behaviour under the mixed-mode I/II load. Subsequently, the experimental results validated the applicability of the DIC technique to the concrete material, which provided the displacements field for the calculation of the WE terms. Furthermore, the experimental part showed that the mixed-mode I/II resistance can be influenced by the aggressive environment.

## 4.7    Fracture Properties and Resistance under Mixed-mode I/II.

The fracture properties were evaluated on the BDCN geometry for various concrete materials and compared between each other. Analysed FMPs were fracture toughness $K_{IC}$ and the critical distance $r_C$ have governing role in the mixed mode I/II fracture resistance. Furthermore, the evaluated fracture resistance curves by the GMTS criterion were presented for each material and compared to the commonly used C 50/60 material.

Generally, it was found that the mixed-mode I/II fracture resistance curve, evaluated by the MTS criterion, shows poor prediction of the specimen failure, while the GMTS curve shows overall better prediction. In addition to this, the GMTS curves are highly

affected by the number of the tests used for the $K_{IC}$ evaluation. Therefore, it is recommended to use more specimens for the $K_{IC}$ testing in the mixed mode I/II fracture analysis. Besides this, the general conclusion can be made, i.e. that with the increasing mechanical and material's fracture mechanical properties the fracture resistance under the mixed mode I/II improves as well.

## 4.8    Influence of Aggressive Environment

The experimental results evaluated on the specimens saturated in chloride solution, showed generally lower value of fracture toughness $K_{IC}$ and lower resistance to the mixed mode I/II loading if compared to the water saturated specimens. The chloride penetration depth was measured by the colorimetric method. The chloride ingress to the specimen body was studied and the effective thickness was calculated. Traditionally, the chloride influence is analysed on the resistance of the reinforcement's corrosion, while in this case of unique study, the results showed, that the chlorides can have major influence on the durability of the concrete itself.

## 5    Perspectives for further Research

This thesis dealt with the mixed mode I/II fracture from various viewpoints, and it can be stated, after finishing it, that it opened even more interesting topics to be investigated. An interesting topic to be studied could be the comparison the DIC displacements fields and the CDP numerically generated ones. This would validate the applicability of the CDP model and bring more insight into the mixed-mode I/II fracture analysis. Furthermore, it would be interesting to compare the *P-CMOS* and *P-CMOD* curves for the DIC and CDP case.

The influence of the aggressive environment on the fracture toughness and fracture resistance under the mixed mode I/II can be extended as well. This analysis could consider progress of the chloride ingress to the concrete body over the time, i.e. from 1 month to 1 year. Furthermore, an advanced screening method could be employed, i.e. tomography, to analyse micro-structure, defects and size of the pores. Also, some microscope technique could be employed to locate the Friedel's salt crystallization and consequent damaging microstructure.

From the LEFM experimental viewpoint, it would be beneficial to find the circular geometry for which the *T*-stress is less than zero. This would lead to improvement of the fracture toughness accuracy and leading into improvement of the GMTS fracture predictions.

# References

[1] M.A. Caldarone, High-Strength Concrete: A Practical Guide, CRC Press, 2019.

[2] P.-C. Aïtcin, R.J. Flatt, Science and technology of concrete admixtures, Woodhead publishing, 2015.

[3] E.G. Nawy, Fundamentals of High-Performance Concrete, Wiley, 2001.

[4] M. Schneider, The cement industry on the way to a low-carbon future, Cement and Concrete Research, 124 (2019) 105792.

[5] S.A. Miller, V.M. John, S.A. Pacca, A. Horvath, Carbon dioxide reduction potential in the global cement industry by 2050, Cement and Concrete Research, 114 (2018) 115-124.

[6] K.E. Hassan, J.G. Cabrera, R.S. Maliehe, The effect of mineral admixtures on the properties of high-performance concrete, Cement and Concrete Composites, 22 (2000) 267-271.

[7] R. Yu, P. Spiesz, H.J.H. Brouwers, Development of an eco-friendly Ultra-High Performance Concrete (UHPC) with efficient cement and mineral admixtures uses, Cement and Concrete Composites, 55 (2015) 383-394.

[8] Q. Tran, P. Ghosh, Influence of pumice on mechanical properties and durability of high performance concrete, Construction and Building Materials, 249 (2020) 118741.

[9] E. Vejmelková, D. Koňáková, T. Kulovaná, M. Keppert, J. Žumár, P. Rovnaníková, Z. Keršner, M. Sedlmajer, R. Černý, Engineering properties of concrete containing natural zeolite as supplementary cementitious material: Strength, toughness, durability, and hygrothermal performance, Cement and Concrete Composites, 55 (2015) 259-267.

[10] J.L. Provis, J.S.J. van Deventer, Alkali Activated Materials: State-of-the-Art Report, RILEM TC 224-AAM, Springer Netherlands, 2013.

[11] J.L. Provis, Alkali-activated materials, Cement and Concrete Research, 114 (2018) 40-48.

[12] J.L. Provis, 4 - Activating solution chemistry for geopolymers, in: J.L. Provis, J.S.J. van Deventer (Eds.) Geopolymers, Woodhead Publishing, 2009, pp. 50-71.

[13] A. McIntosh, S.E.M. Lawther, J. Kwasny, M.N. Soutsos, D. Cleland, S. Nanukuttan, Selection and characterisation of geological materials for use as geopolymer precursors, Advances in Applied Ceramics, 114 (2015) 378-385.

[14] S. Donatello, O. Maltseva, A. Fernandez-Jimenez, A. Palomo, The Early Age Hydration Reactions of a Hybrid Cement Containing a Very High Content of Coal Bottom Ash, Journal of the American Ceramic Society, 97 (2014) 929-937.

[15] M.A. Longhi, E.D. Rodríguez, S.A. Bernal, J.L. Provis, A.P. Kirchheim, Valorisation of a kaolin mining waste for the production of geopolymers, Journal of Cleaner Production, 115 (2016) 265-272.

[16] Eurocode 2: Design of concrete structures—Part 1-1: General rules and rules for buildings, Brussels, Belgium, (2004).

[17] AASHTO LRFD bridge design specifications, Transportation (Amst). Washington, DC, (2007).

[18] Model Code 2010 First complete draft, Bulletin, 55 (2010).

[19] E.O.L. Lantsoght, C. van der Veen, A. de Boer, Proposal for the fatigue strength of concrete under cycles of compression, Construction and Building Materials, 107 (2016) 138-156.

[20] M.K. Lee, B.I.G. Barr, An overview of the fatigue behaviour of plain and fibre reinforced concrete, Cement and Concrete Composites, 26 (2004) 299-305.

[21] S. Korte, V. Boel, W. De Corte, G. De Schutter, Behaviour of fatigue loaded self-compacting concrete compared to vibrated concrete, Structural Concrete, 15 (2014) 575-589.

[22] C. Gaedicke, J. Roesler, S. Shah, Fatigue crack growth prediction in concrete slabs, International Journal of Fatigue, 31 (2009) 1309-1317.

[23] R. François, S. Laurens, F. Deby, Corrosion and its Consequences for Reinforced Concrete Structures, ISTE Press - Elsevier, 2018.

[24] Z.-H. Lu, Y.-G. Zhao, Z.-W. Yu, F.-X. Ding, Probabilistic evaluation of initiation time in RC bridge beams with load-induced cracks exposed to de-icing salts, Cement and Concrete Research, 41 (2011) 365-372.

[25] M.G. Stewart, D.V. Rosowsky, Time-dependent reliability of deteriorating reinforced concrete bridge decks, Structural Safety, 20 (1998) 91-109.

[26] B. Teplý, M. Chromá, P. Rovnaník, Durability assessment of concrete structures: reinforcement depassivation due to carbonation, Structure and Infrastructure Engineering, 6 (2010) 317-327.

[27] B. Teplý, D. Vorechovská, Reinforcement Corrosion: Limit States, Reliability and Modelling, Journal of Advanced Concrete Technology, 10 (2012) 353-362.

[28] M. Kušter Marić, J. Ožbolt, G. Balabanić, Reinforced concrete bridge exposed to extreme maritime environmental conditions and mechanical damage: Measurements and numerical simulation, Engineering Structures, 205 (2020) 110078.

[29] L. Yu, R. François, V.H. Dang, V. L'Hostis, R. Gagné, Structural performance of RC beams damaged by natural corrosion under sustained loading in a chloride environment, Engineering Structures, 96 (2015) 30-40.

[30] F.H. Wittmann, K. Rokugo, E. Brühwiler, H. Mihashi, P. Simonin, Fracture energy and strain softening of concrete as determined by means of compact tension specimens, Materials and Structures, 21 (1988) 21-32.

[31] Rilem, Recommendation, Determination of the fracture energy of mortar and concrete by means of three-point bend tests on notched beams, Materials and structures, 18 (1985) 285-290.

[32] European, Committee, for, Standardization, EN 12390-5  Testing hardened concrete in:  Part 5: Flexural strength of test specimenes, European Committee for Standardization, 2009, pp. 12.

[33] H. Linsbauer, E. Tschegg, Fracture energy determination of concrete with cube-shaped specimens, Zement und Beton, 31 (1986) 38-40.

[34] L. Malíková, V. Veselý, S. Seitl, Estimation of the crack propagation direction in a mixed-mode geometry via multi-parameter fracture criteria, Frattura ed Integrità Strutturale, (2015) 25.

[35] J.C. Gálvez, M. Elices, G.V. Guinea, J. Planas, Mixed Mode Fracture of Concrete under Proportional and Nonproportional Loading, International Journal of Fracture, 94 (1998) 267-284.

[36] D. Li, L.N.Y. Wong, The Brazilian Disc Test for Rock Mechanics Applications: Review and New Insights, Rock Mechanics and Rock Engineering, 46 (2013) 269-287.

[37] C. Atkinson, R.E. Smelser, J. Sanchez, Combined mode fracture via the cracked Brazilian disk test, International Journal of Fracture, 18 (1982) 279-291.

[38] M. Abshirini, N. Soltani, P. Marashizadeh, On the mode I fracture analysis of cracked Brazilian disc using a digital image correlation method, Optics and Lasers in Engineering, 78 (2016) 99-105.

[39] M.R.M. Aliha, M.R. Ayatollahi, Two-parameter fracture analysis of SCB rock specimen under mixed mode loading, Engineering Fracture Mechanics, 103 (2013) 115-123.

[40] J. Akbardoost, M.R. Ayatollahi, M.R.M. Aliha, M.J. Pavier, D.J. Smith, Size-dependent fracture behavior of Guiting limestone under mixed mode loading, International Journal of Rock Mechanics and Mining Sciences, 71 (2014) 369-380.

[41] M.R.M. Aliha, M.R. Ayatollahi, Mixed mode I/II brittle fracture evaluation of marble using SCB specimen, Procedia Engineering, 10 (2011) 311-318.

[42] M. Moazzami, M.R. Ayatollahi, H.R. Chamani, M. Guagliano, L. Vergani, Determination of higher order stress terms in cracked Brazilian disc specimen under mode I loading using digital image correlation technique, Optics & Laser Technology, 107 (2018) 344-352.

[43] A.A. Griffith, G.I. Taylor, VI. The phenomena of rupture and flow in solids, Philosophical Transactions of the Royal Society of London. Series A, Containing Papers of a Mathematical or Physical Character, 221 (1921) 163-198.

[44] G.R. Irwin, Analysis of stresses and strains near the end of a crack traversing a plate, Journal of Applied Mechanics, 24 (1957) 361-364.

[45] M.L. Williams, On the Stress Distribution at the Base of a Stationary Crack, Journal of Applied Mechanics, 24 (1956) 6.

[46] M. Williams, The bending stress distribution at the base of a stationary crack, J Appl Mech, 24 (1957) 109-114.

[47] L.P. Pook, Linear Elastic Fracture Mechanics for Engineers: Theory and Applications, WIT Press, 2000.

[48] T.L. Anderson, Fracture mechanics: fundamentals and applications, CRC press, 2017.

[49] B.L. Karihaloo, Fracture Mechanics and Structural Concrete (Concrete Design and Construction Series), Ed. Longman Scientific & Technical. United States, (1995).

[50] H.T. Nguyen, M. Pathirage, G. Cusatis, Z.P. Bažant, Gap Test of Crack-Parallel Stress Effect on Quasibrittle Fracture and Its Consequences, Journal of Applied Mechanics, 87 (2020).

[51] Z.P. Bažant, Mechanics of fracture and progressive cracking in concrete structures, in: Fracture mechanics of concrete: Structural application and numerical calculation, Springer, Dordrecht, The Netherlands, 1985, pp. 1-94.

[52] Z.P. Bažant, Concrete fracture models: testing and practice, Engineering Fracture Mechanics, 69 (2002) 165-205.

[53] H. Mihashi, N. Nomura, S. Niiseki, Influence of aggregate size on fracture process zone of concrete detected with three dimensional acoustic emission technique, Cement and Concrete Research, 21 (1991) 737-744.

[54] F. Erdogan, G.C. Sih, On the Crack Extension in Plates Under Plane Loading and Transverse Shear, Journal of Basic Engineering, 85 (1963) 519-525.

[55] G.C. Sih, Strain-energy-density factor applied to mixed mode crack problems, International Journal of Fracture, 10 (1974) 305-321.

[56] J. Qian, A. Fatemi, Mixed mode fatigue crack growth: A literature survey, Engineering Fracture Mechanics, 55 (1996) 969-990.

[57] M.R. Ayatollahi, M. Rashidi Moghaddam, F. Berto, A generalized strain energy density criterion for mixed mode fracture analysis in brittle and quasi-brittle materials, Theoretical and Applied Fracture Mechanics, 79 (2015) 70-76.

[58] M.R. Ayatollahi, M. Rashidi Moghaddam, F. Berto, T-stress effects on fatigue crack growth – Theory and experiment, Engineering Fracture Mechanics, 187 (2018) 103-114.

[59] D.J. Smith, M.R. Ayatollahi, M.J. Pavier, The role of T-stress in brittle fracture for linear elastic materials under mixed-mode loading, Fatigue & Fracture of Engineering Materials & Structures, 24 (2001) 137--150.

[60] M.R. Ayatollahi, M.R.M. Aliha, On the use of Brazilian disc specimen for calculating mixed mode I-II fracture toughness of rock materials, Engineering Fracture Mechanics, 75 (2008) 4631-4641.

[61] G.R. Irwin, Plastic Zone Near a Crack and Fracture Toughness., in: Sagamore Research Conference, 1961, pp. 63-78.

[62] H. Tada, P.C. Paris, G.R. Irwin, American Society of Mechanical Engineers., ASM International., The stress analysis of cracks handbook, 3rd ed., ASME Press : Professional Engineering Pub. : ASM International, New York, 2000.

[63] S. Seitl, P. Miarka, V. Bílek, The mixed-mode fracture resistance of C 50/60 and its suitability for use in precast elements as determined by the Brazilian disc test and three-point bending specimens, Theoretical and Applied Fracture Mechanics, 97 (2018) 108-119.

[64] Abaqus, Analysis User's Manual 6.14, Dassault Systemes Simulia Corp.,(2011).

[65] S. Seitl, P. Miarka, V. Bílek, The Mixed-Mode Fracture Resistance of C 50/60 and its Suitability for Use in Precast Elements as Determined by the Brazilian Disc Test and Three-Point Bending Specimens, Theoretical and Applied Fracture Mechanics, (2018).

[66] NT BUILD 492 Concrete, mortar and cement-based repair materials:, in: Chloride migration coefficient from non-steady-state migration experiments, NORDTEST, Espoo, Finland, 1999.

[67] X. Qian, Z. Li, The relationships between stress and strain for high-performance concrete with metakaolin, Cement and Concrete Research, 31 (2001) 1607-1611.

# About Author

Petr Miarka
Institute of Structural Mechanics
Faculty of Civil Engineering
Brno University of Technology
Veveří 331/95, 602 00 Brno
Czech Republic

Email: Petr.Miarka@vut.cz

# Education

| | |
|---|---|
| Since 02/2017 | Ph.D. student (4$^{th}$ year), Brno University of Technology, Faculty of Civil Engineering, Institute of Structural Mechanics, |
| 01/2017 | **Ing.**, Brno University of Technology, Faculty of Civil Engineering. |
| 06/2014 | **Bc.**, Brno University of Technology, Faculty of Civil Engineering. |

# Practical Experience

| | |
|---|---|
| Since 01/2017 | **Institute of Physics of Materials,** Academy of Science of the Czech Republic, (IPM ASCR), Žižkova 22, Brno – Ph.D. student |
| | Brno University of Technology, Faculty of Civil Engineering, **Institute of Structural Mechanics** (ISM FCE BUT) – Assistant lecturer |

# International Internships

| | |
|---|---|
| 02-08/2018 | Traineeship via Erasmus+, **Ghent University**, Ghent, Belgium (Prof. Wouter De Corte) |
| 11/2017 | Study internship via Freemovers+ mobility programme, , **University of Seville**, Seville, Spain (Assoc. prof. Héctor Cifuentes Bulté) |

# Teaching Experience

Teaching basic topics from structural mechanics at FCE BUT.

BD001 – Fundamentals of Structural Mechanics, BD004 – Statics II. Since 2017 - supervision of Bachelor's and Master's thesis (currently > 8 students)

# Grants and Participation in Research Projects

| | |
|---|---|
| **Brno PhD Talent** | Brno PhD Talent scholarship holder funded by Brno city municipally and South Moravian Centre for International Mobility. Period of funding 2018-2021. |
| **BUT internal grant agency**. | **FAST-J-20-6341, FAST-J-19-5783, FAST-J-18-5164, FAST-S-20-6278, FAST-S-19-5896, and FAST-S-18-5614** |
| **Czech Science Foundation.** | **20-00761S, 18-12289Y, 17-01589S, 16-18702S** |

# Awards

**CONFERENCE ATTENDANCE AWARD 2018** on 18th International Conference on Experimental Mechanics in Brussel Belgium, 1st-5th July 2018
organized by **The European Society for Experimental Mechanics.**

# Software Skills

| | |
|---|---|
| Office software: | **Microsoft Office** (Word, Excel, PowerPoint), Adobe **Photoshop**, Autodesk **AutoCAD**, **Inscape.** |
| Software for structural analysis | **Dlubal – RFEM 5.0** and **Nemetschek – Scia Engineer**: FEM software for design of civil engineering structures according to Eurocodes |
| | **Simulia ABAQUS**: advanced FEM software or design of civil engineering structures (static linear/non-linear analysis), |
| | **ANSYS Mechanical APDL**: Certified user after workshop by SVS FEM (November 2017): ANSYS Mechanical APDL-1,2 ANSYS Mechanical APDL – Dynamics. |
| | **Matlab** Certified user after workshop by HUMUSOFT (September 2018 and November 2019) |

# List of Selected Papers

Complete list of author's publications:

https://www.vutbr.cz/en/people/petr-miarka-135903

**MIARKA, P., SEITL, S., LEHNER, P., HORNAKOVA, M., KONEČNÝ, P., SUCHARDA, O., BÍLEK, V.,** Influence of Chlorides on the Fracture Toughness and Fracture Resistance Under the Mixed Mode I/II of High-Performance Concrete. *Theoretical and Applied Fracture Mechanics*, 2020, vol.110, 102812, pp. 1-15. ISSN: 0167-8442. DOI: 10.1016/j.tafmec.2020.102812 **IF**: 3.021 Q1/Q2

**MIARKA, P.,** PAN, L., BÍLEK, V., SEITL, S., CIFUENTÉS, H., Influence of the Chevron Notch Type on the Values of Fracture Energy Evaluated on Alkali-Activated Concrete. *Engineering Fracture Mechanics*, 2020, vol. 236, 107209, pp. 1-18. DOI: 10.1016/j.engfracmech.2020.107209 **IF**: 3.426 Q1

**MIARKA, P.,** CRUCES, A., SEITL, S., MALÍKOVÁ, L., LOPÉZ-CRESPO, P., Evaluation of the SIF and T-stress values of the Brazilian disc with a central notch by hybrid method. *International Journal of Fatigue*, 2020, vol. 135, no. 1, pp. 1-12. ISSN: 0142-1123. DOI: 10.1016/j.ijfatigue.2020.105562 **IF**: 4.369, Q1/Q2

**MIARKA, P.,** CRUCES, A., SEITL, S., MALÍKOVÁ, L., LOPÉZ-CRESPO, P., Influence of the constraint effect on the fatigue crack growth rate in S355 J2 steel using digital image correlation. *Fatigue and Fracture of Engineering Materials and Structures*, 2020, vol. 43, no. 8, pp. 1703-1718. ISSN: 1460-2695. DOI: 10.1111/ffe.13198 **IF**: 3.031 Q1/Q2

**MIARKA, P**., SEITL, S., DE CORTE, W. Notch Tip Displacements of the Concrete Brazilian Disc Test with Central Notch Analysed by the Concrete Damaged Plasticity Model. *Theoretical and Applied Fracture Mechanics*, 2019, vol. 102, no. 1, pp. 122-150. ISSN: 0167-8442. DOI: 10.1016/j.tafmec.2019.04.006 **IF**: 3.021 Q1/Q2

SEITL, S., **MIARKA, P.,** BÍLEK, V., The Mixed-Mode Fracture Resistance of C 50/60 and its Suitability for Use in Precast Elements as Determined by the Brazilian Disc Test and Three-Point Bending Specimens. *Theoretical and Applied Fracture Mechanics*, 2018, vol. 2018, no. 97, pp. 108-119. ISSN: 0167-8442. DOI: 10.1016/j.tafmec.2018.08.003 **IF**: 3.021 Q1/Q2

**MIARKA, P.** SEITL, S. BÍLEK, V. Mixed-mode fracture analysis in High-performance concrete using brazilian disc test. *Materiali in tehnologije*, 2019, vol. 53, no. 2, pp. 233-238. ISSN: 1580-2949. DOI: 10.17222/mit.2018.161 **IF**: 0.697 Q4